ISSN 1590-2595
Anno 2013_Numero 105

The March 11th, 2011, M 9.0 earthquake offshore Honshu island (Japan): a synthesis of the Tohoku-Oki INGV Team research activities

Quaderni di Geofisica

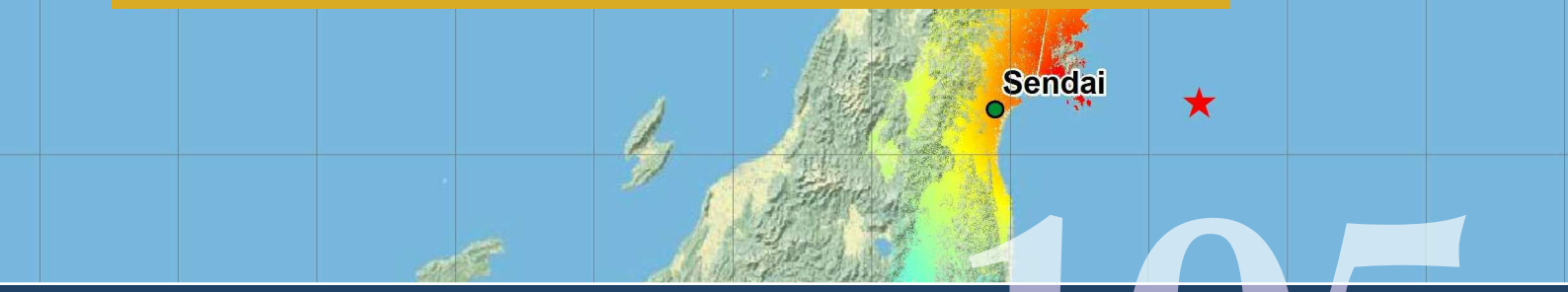

105

Istituto Nazionale di
Geofisica e Vulcanologia

Quaderni di Geofisica

Segreteria di Redazione
Francesca Di Stefano - coordinatore
Tel. +39 06 51860068
Fax +39 06 36915617
Rossella Celi
Tel. +39 06 51860055
Fax +39 06 36915617

redazionecen@ingv.it

ISSN 1590-2595
Anno 2013_Numero 105

The March 11th, 2011, M 9.0 earthquake offshore Honshu island (Japan): a synthesis of the Tohoku-Oki INGV Team research activities

Il terremoto dell'11 marzo 2011, M 9.0, al largo dell'isola di Honshu (Giappone): sintesi delle attività di ricerca del Tohoku-Oki INGV Team

Tohoku-Oki INGV Team composition:

Stefania Amici[1], Marco Anzidei[1], Christian Bignami[1], Carlo Alberto Brunori[1], Sven Borgstrom[2], Fabrizia Buongiorno[1], Daniele Cheloni[1], Marco Chini[1], Francesca R. Cinti[3], Nicola D'Agostino[1], Paolo Marco De Martini[3], Alessio Fornaciai[4], Salvo Gambino[5], Francesco Guglielmino[5], Christodoulos Kyriakopoulos[1], Stefano Lorito[3], Daniele Melini[3], Luca Merucci[1], Marco Moro[1], Rosa Nappi[2], Daniela Pantosti[3], Alessio Piatanesi[3], Alessandro Piscini[1], Giuseppe Puglisi[5], Federica Riguzzi[1], Fabrizio Romano[3], Malvina Silvestri[1], Valeria Siniscalchi[2], Salvatore Stramondo[1]

[1]**INGV** (Istituto Nazionale di Geofisica e Vulcanologia, Centro Nazionale Terremoti)
[2]**INGV** (Istituto Nazionale di Geofisica e Vulcanologia, Sezione di Napoli - Osservatorio Vesuviano)
[3]**INGV** (Istituto Nazionale di Geofisica e Vulcanologia, Sezione Sismologia e Tettonofisica)
[4]**INGV** (Istituto Nazionale di Geofisica e Vulcanologia, Sezione di Pisa)
[5]**INGV** (Istituto Nazionale di Geofisica e Vulcanologia, Sezione di Catania - Osservatorio Etneo)

In copertina Mappa di spostamento ENVISAT. L'epicentro del terremoto dell'11 marzo 2011 è indicato dalla stella rossa (particolare)

The March 11th, 2011, M 9.0 earthquake offshore Honshu island (Japan): a synthesis of the Tohoku-Oki INGV Team research activities

On March 11th, 2011 (at 05:46:23 UTC) a megaearthquake (M 9.0) occurred near the NE coast of Honshu island (Japan), originated near the subduction plate boundary between the Pacific and the North America plates. The epicenter has been located at about 130 km East of Sendai city, at a depth of about 32 km. This seismic event has been followed by a devastating tsunami. The location, the geometric parameters, the focal mechanism, are in agreement with the occurrence of the earthquake along the subduction plate boundary. The initial seismological analysis indicated that a surface of about 300 km x 150 km over the fault moved upwards of 30-40 m. The Tohoku-Oki INGV Team has made available a wide and multisciplinary expertise to investigate the different scientific issues concerning the earthquake. Indeed from Seismology to Geomorphology, from Remote Sensing to GPS, from Tsunami to Source Modeling the INGV Team has completed a wide range of analysis, obtaining relevant outcomes that are summarized in this work.

L'11 Marzo 2011 (05:46:23 UTC) un sisma di eccezionale magnitude (9.0) ha avuto luogo in prossimità della costa dell'isola di Honshu in Giappone, originatosi presso l'area in subduzione lungo il margine di placca Pacifica e Nord Americana. L'epicentro è stato localizzato a circa 130 km ad est di Sendai e ad una profondità di circa 32 km. Il sisma è stato seguito da un devastante tsunami. La localizzazione, i parametri geometrici, il meccanismo focale, tutti sono in accordo con il verificarsi di un sisma lungo tale margine di placca. Le prime analisi sismologiche hanno indicato che una superficie di circa 300 km x 150 km si è sollevata di 30-40 m. Il Tohoku-Oki INGV Team ha messo a disposizione un vasto range di competenze in differenti ambiti scientifici che hanno consentito di analizzare una ampia varietà e quantità di dati. Infatti il Team INGV ha effettuato analisi sismologiche, geomorfologiche, da dati Telerilevati e GPS, inerenti lo tsunami e la modellazione della sorgente sismica. La sintesi di tali attività e i risultati sono presentati in questo lavoro.

Introduction

The March 11, 2011 (at 05:46:23 UTC) megaearthquake (M 9.0) has been the strongest seismic event of the recent years in the world, except for the December 26, 2004, M 9.3, Indonesia earthquake. The East coast of Honshu, the main island of Japanese archipelago, has been affected by the coseismic shaking and surface deformation, and by the tsunami wave. This latter has provoked most of the damages on land and in particular to the infrastructures in the urbanized regions.

The so called Tohoku-Oki earthquake can be easily considered the most investigated seismic event in terms of number and variety of satellite data and sensors, in terms of available geodetic-GPS stations, and in terms of multidisciplinary approaches performed to merge such data.

It is worth noting that thanks to its exceptionality, the Tohoku-Oki earthquake has some major scientific open issues till now, concerning, for instance, the maximum expected magnitude of a seismogenic fault and the unexpected height of the tsunami wave. Further studies are ongoing, and further results are now in press. However the aim of this paper is to provide an overview of the data, the processing techniques and the methodologies that have lead to the results here presented.

The activities have been organized in sub-teams based on the

different expertise available at INGV. So, as it is shown later, this report focuses on the results obtained in the framework of the Tohoku-Oki INGV Team that mainly concern the following topics:

- surface deformation pattern from DInSAR
- the coastal impact of the Tsunami induced by the earthquake
- seismic source modeling
- tide gauge analysis

The measurement of "surface deformation from DInSAR" has provided a clear view of the displacements all over Honshu island and in particular along the coastal regions. The "impact of the Tsunami" has been investigated by satellite image combination in order to provide a synoptic picture of the effects on land of the Tsunami wave. Some of the outcomes have been processed by seismic source inversion procedures to obtain a model of the seismogenic "structure" offshore where the earthquake occurred. Finally, more specific analyses have been addressed to investigate the role of the "tide gauge" elsewhere, at large distance from the epicentral region.

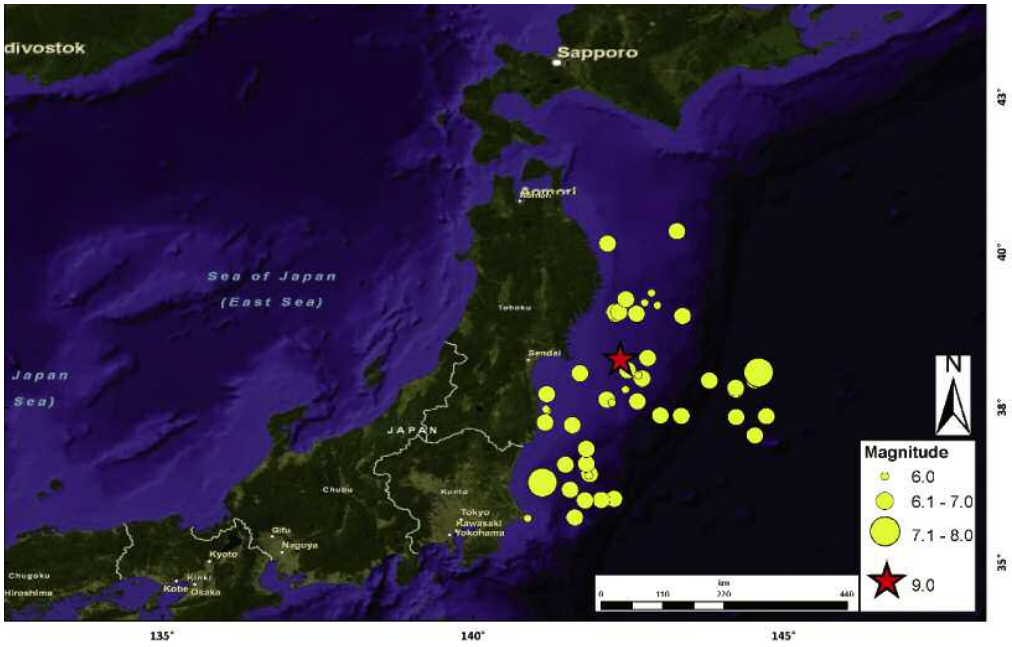

Figure 1 Map of the March 11, 2011, epicenter and the aftershocks with M>6.
Figura 1 Epicentro del terremoto dell'11 marzo 2011 e degli aftershocks con M>6.

1. The "Tohoku-Oki INGV Team"

The worldwide resonance of the March 11th earthquake spontaneously moved a lot of Earth Scientists to investigate this exceptional event, to detect and measure the surface effects, to model the seismic source and to explain the causes. The wish to provide a contribution has *contaminated* a group of researchers at INGV. The initiative, totally on voluntary basis, collected around a table about 30 people from most of INGV sites, Rome, Napoli, Catania, Palermo, Pisa. The *Tohoku-Oki INGV Team* has joined around common topics the different scientific and technical capabilities present at INGV. From Seismology to Geomorphology, from Remote Sensing to GPS, from Tsunami to Source Modeling, the *Tohoku-Oki INGV Team* has simply demonstrated once again how wide is the spread of skills available at INGV.
Due to its specific origin, that has its starting point in the will to collaborate to the investigation of the wide range of "signals", this paper is a collection of results not necessarily connected. Indeed, although the *Tohoku-Oki INGV Team* has had a common scope, the knowhow and the technical capabilities of each group have lead to obtain outcomes not ever linked among each other. This simply means that the *Team* has worked in parallel to investigate different aspects of the same problems, each one using specific data and tools.
Finally, our wish is that the initiative that lead to have the *Tohoku-Oki INGV Team* might be the basis of an organized group of researchers at INGV able to provide a structured feedback in case of forthcoming international disasters.

2. The March 11, 2011 earthquake and tsunami: overview

The disastrous earthquake (M 9.0) occurred on March 11th, 2011 (at 05:46:23 UTC) near the NE coast of Honshu island (Japan) originated near the subduction plate boundary between the Pacific and the North America plates. The epicenter is at about 130 km East of Sendai city, at a depth of about 32 km. The location, the geometric parameters, the focal mechanism, are in agreement with the occurrence of the seism along the subduction plate boundary. The initial seismological analysis indicated that a surface of about 300 km x 150 km over the fault moved upwards of 30-40 m. The mainshock followed some large foreshocks starting two days before, March 9 with a M 7.2 about 40 km from the epicenter of the main event, besides other three earthquakes over M 6.
The movement of the Pacific plate with respect to the North America is about 83 mm/y in this area.
The Japan Trench since 1973 has hosted nine events of M 7 or greater, the largest of which was a M 7.8 located about

260 km N of March 11th epicenter. Later on in June 1978 a M 7.7 took place 35 km SW of March 11th 2011.
The northern portion of the coast of Honshu has been hit by tsunamis too. In particular following the M 7.6 subduction earthquake in 1896, waves up to 38 m were measured. Later on, the M 8.6 event of March 2, 1933, generated waves of 29 m height on the Sankiru coast.
The March 11, 2011 earthquake far surpassed other post-1900 plate-boundary thrust-fault earthquakes in the southern Japan Trench, none of which reached M8. A predecessor may have occurred on July 13, 869, when the Sendai area was swept by a large tsunami that Japanese scientists have identified from written records and from a sand sheet.

3. Co-seismic displacement field and source modeling

3.1 Mapping displacement field from SAR Interferometry

Soon after the earthquake, some of the most important Space Agencies made available their data all over the epicentral region. JAXA (Japanese Space Agency), ESA (European Space Agency), DLR (German Space Agency), NASA (National Aero Space Agency) and CNES (French Space Agency) provided a large number of SAR and Optical images. Each Agency has applied a different policy for data delivery, ranging from ESA and JAXA that freely opened the databases for Japan earthquake, up to CNES and DLR that made available their data conditioned to a registration.
The INGV Team coordinated the efforts and shared the satellite data to minimize the time for processing. More in detail, concerning SAR sensors, the ENVISAT and ALOS data.

3.1.1 ENVISAT data processing

Three interferometric pairs of ENVISAT strips have been processed. They are composed of 13 frames on track 347, 8 frames on track 074 and 6 frames on track 189. The ENVISAT images are all in IS6 acquisition mode, which is characterized by an incidence angle of 40° at center swath and with a pixel resolution of 25m. All the tracks are on descending orbit. The interferograms (Fig. 2) covers most of Honshu island, the whole epicentral region and a large coastal area for a total of about 800x200 Km. Table 1 summarizes the dates and spatial baselines of the processed images.The interferograms have been processed to obtain a fringe map at 40m per pixel resolution, i.e. by applying a multi-look factor of 2 looks x 10 looks in range and azimuth respectively. Finally, the whole strips have been unwrapped to measure the LOS surface movement (Fig. 3). The

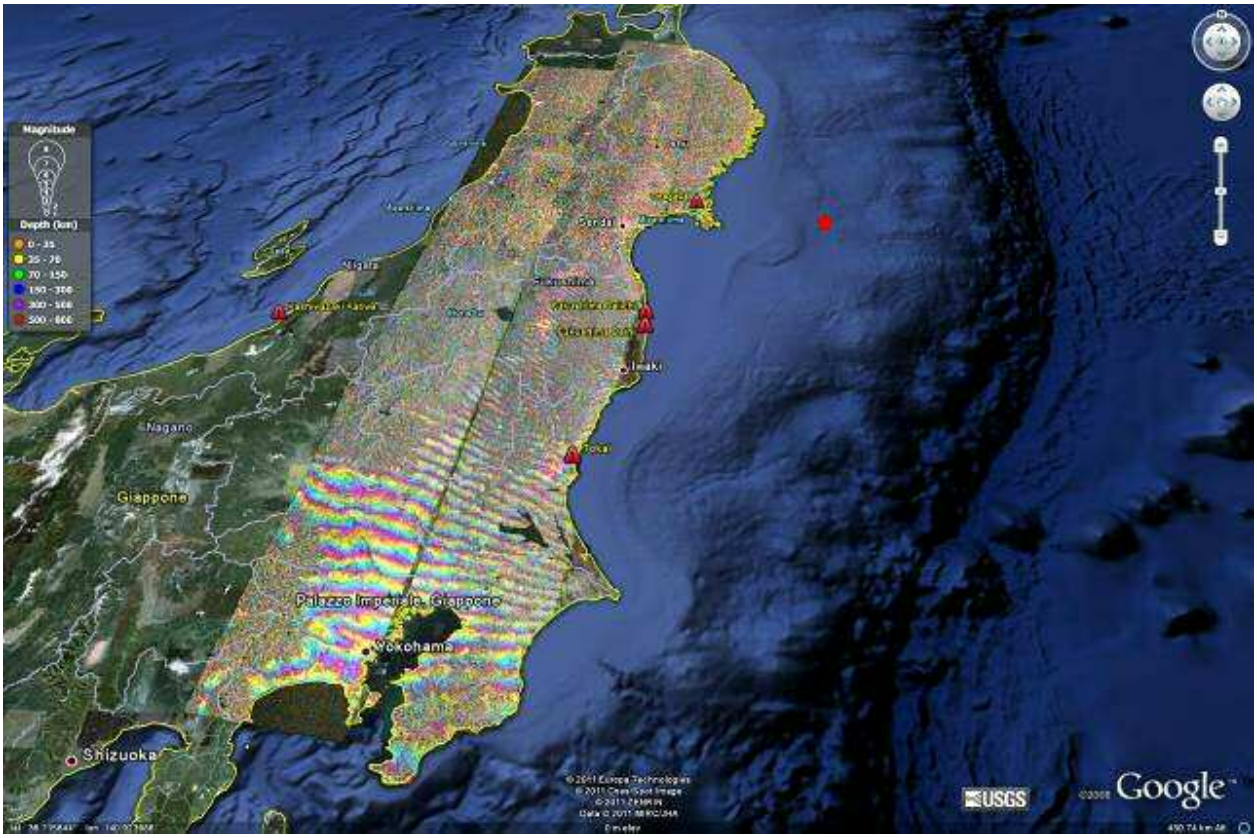

Figure 2 3D view of the interferograms resulting from the mosaic of three ENVISAT tracks. The red star indicates the epicenter of the mainshock of March 11 (Mw 9.0). Red triangles are the nuclear power plants.
Figura 2 Vista 3D degli interferogrammi ottenuti dal mosaic di tre track ENVISAT. L'epicentro del terremoto dell'11 marzo 2011 è indicato dalla stella rossa. I triangoli verdi sono le centrali nucleari.

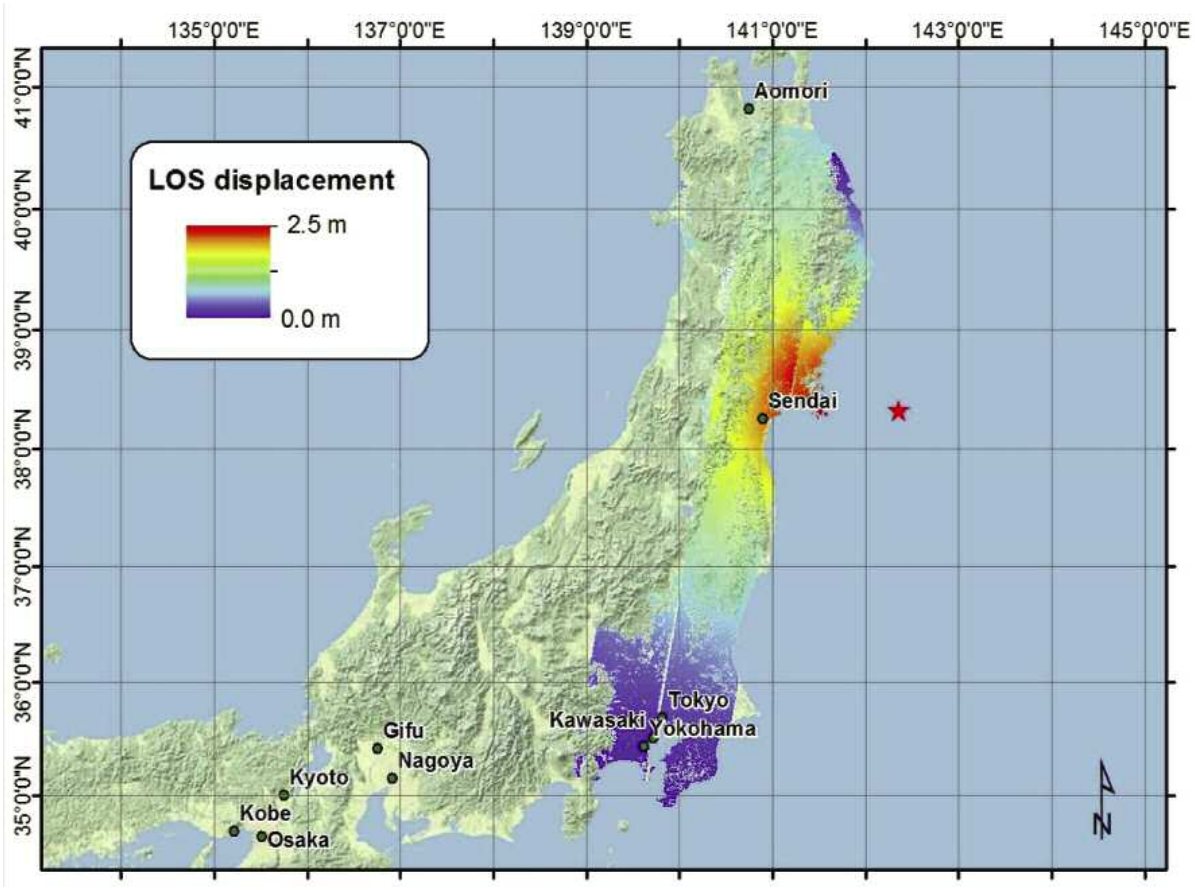

Figure 3 Unwrapped, geo-coded and mosaic of the ENVISAT data. The red star indicates the epicenter.
Figura 3 Mappa di spostamento ENVISAT srotolata, geocodificata e mosaicata. L'epicentro è indicato dalla stella rossa.

retrieved surface deformation shows a maximum displacement that reaches about 2.5 m, relative to a reference point within the entire frames located nearby the southern boundary, in the coastal area close to Sendai city.

3.1.2 ALOS data processing

The PALSAR sensor on board of ALOS acquired two adjacent tracks in FBS (Fine Beam Single) and FBD (Fine Beam Double) polarization. The data processing was carried out using ROI_PAC 3.0.1 *(Repeat Orbit Interferometry PACkage)* from JPL (Jet Propulsion Laboratory, USA). The time span of track 401 paris is 28/10/2010-15/3/2011, and for track 402 it is 29/9/2010-1/4/2011. Fig. 4a and Fig. 4b show the interferograms from ascending tracks 401 and 402 respectively. Each colour cycle represents 11.8 cm of deformation into the radar line of sight (LOS). Fig. 4c is the combination of the two tracks. As a general remark, we observe that, in spite of the L band of the ALOS-PALSAR sensor, which is usually less affected by vegetation or other decorrelation sources, showing good coherence over time, the two pairs are somewhere decorrelated, likely due to the presence of vegetation or also snow over the innermost mountainous areas. Probably, also the atmospheric effects cannot be neglected.

Track	Dates	Baseline [m]
074	02/03/2011 – 01/04/2011	168
189	08/02/2011 – 09/04/2011	509
347	19/02/2011-21/03/2011	206

Table 1 Tracks, dates and spatial baseline of the ENVISAT interferometric pairs.
Tabella 1 Tracks, date e baseline spaziale delel coppie interferometriche ENVISAT.

3.2 GPS and InSAR data integration

In this section we describe the retrival of the 3D displacements carried out by integrating GPS and InSAR results. We adopt the SISTEM method for estimating the gradient displacements tensor [Guglielmino et al., 2011]. SISTEM takes into account both the in situ geodetic measurements and the DinSAR LOS displacement maps. In this case, we integrated the GPS displacement vectors provided in section 4.3, obtained by comparing the position estimates averaged 15 minutes before and after the main shock, and the ENVISAT

DInSAR displacement map relevant to the Track 347 (on descending orbit) obtained considering the passes of 19/2/2011 and 21/3/2011.

In the following, we shortly describe the mathematical background of the SISTEM approach. A number K of InSAR interferograms can be related to the components of the displacement vector of an arbitrary point P according to the following equation:

$$D_{LOS}^{SP} = [U_1, U_2, U_3]\left[S_x^{SP}, S_y^{SP}, S_z^{SP}\right]^T \quad (1)$$

where D_{LOS}^{SP} are the know LOS displacements maps defined on a grid of N points, where S=1...K, the terms U1, U2 and U3 are the unknown displacements vector components of an arbitrary point P, and $\left[S_x^{SP}, S_y^{SP}, S_z^{SP}\right]$ are the unit vectors pointing from the point P toward the different satellite line of sight.

In order to integrate GPS and DinSAR dataset, we resolve a linear system of the kind $Al = u$ using the Weighted Least Squares (WLS) approach, and we proposed the Design Matrix A, the Observation vector u, and the column vector of unknown parameters l according to the following equations:

$$A = \begin{bmatrix}
1 & 0 & 0 & \Delta x_{1(1)} & \Delta x_{2(1)} & \Delta x_{3(1)} & 0 & 0 & 0 & 0 & \Delta x_{3(1)} & -\Delta x_{2(1)} \\
0 & 1 & 0 & 0 & \Delta x_{1(1)} & 0 & \Delta x_{2(1)} & \Delta x_{3(1)} & 0 & -\Delta x_{3(1)} & 0 & \Delta x_{1(1)} \\
0 & 0 & 1 & 0 & 0 & \Delta x_{1(1)} & 0 & \Delta x_{2(1)} & \Delta x_{3(1)} & \Delta x_{2(1)} & -\Delta x_{1(1)} & 0 \\
. & . & . & . & . & . & . & . & . & . & . & . \\
. & . & . & . & . & . & . & . & . & . & . & . \\
. & . & . & . & . & . & . & . & . & . & . & . \\
1 & 0 & 0 & \Delta x_{1(N)} & \Delta x_{2(N)} & \Delta x_{3(N)} & 0 & 0 & 0 & 0 & \Delta x_{3(N)} & -\Delta x_{2(N)} \\
0 & 1 & 0 & 0 & \Delta x_{1(N)} & 0 & \Delta x_{2(N)} & \Delta x_{3(N)} & 0 & -\Delta x_{3(N)} & 0 & \Delta x_{1(N)} \\
0 & 0 & 1 & 0 & 0 & \Delta x_{1(N)} & 0 & \Delta x_{2(N)} & \Delta x_{3(N)} & \Delta x_{2(N)} & -\Delta x_{1(N)} & 0 \\
S_x^{(1)P} & S_y^{(1)P} & S_z^{(1)P} & 0 & 0 & 0 & 0 & 0 & 0 & 0 & 0 & 0 \\
. & . & . & . & . & . & . & . & . & . & . & . \\
S_x^{(K)P} & S_y^{(K)P} & S_z^{(K)P} & 0 & 0 & 0 & 0 & 0 & 0 & 0 & 0 & 0
\end{bmatrix} \quad (2)$$

where xj(n)=xj(n)-xj0 are the components of the vector distance between the arbitrary point P and the actual GPS benchmark; the measured data vector assumes the form:

$$u = \left[u_{1(1)} u_{2(1)} u_{3(1)} \ldots u_{1(n)} u_{2(n)} u_{3(n)} D_{LOS}^{1P} \ldots D_{LOS}^{KP}\right]^T \quad (3)$$

while the column vector of unknown parameters usually referring to displacement vectors measured at N geodetic benchmarks is:

$$\mathbf{l} = [U_1\ U_2\ U_3\ \varepsilon_{11}\ \varepsilon_{12}\ \varepsilon_{13}\ \varepsilon_{22}\ \varepsilon_{23}\ \varepsilon_{33}\ \omega_1\ \omega_2\ \omega_3]^T \quad (4)$$

It should be observed that the A matrix consists of 3N+K rows: the first 3N rows can be viewed as N blocks of three equations which represent information on the GPS position of each single node of the grid with respect to the arbitrary point P, while the last K equations refers to the corresponding DInSAR data.

In Fig. 5, the U1, U2 and U3 (i.e. North East and Up) components are shown. The SISTEM result evidences that the displacement filed is characterized by a prevalent horizontal component (with about 3.5 - 4 m).The vertical displacement highlights a general upwelling, along a NNE-SSW direction, with a local subsidence, possibly due to landslides or local instabilities.

3.3 GPS Japanese network data and tsunami waveforms solutions

The Tohoku-Oki earthquake ruptured the interface between the Pacific and North America plates, and generated a huge tsunami that devastated parts of the north-eastern Honshu Island for up to 5 km inland. As has been pointed out above, this is probably the best instrumentally recorded great earthquake ever. In fact, in addition to satellite data, the extraordinarily dense Japanese network provided a huge amount of seismological and geodetic information. In this work we perform a joint inversion of available tsunami waveforms and GPS data to infer the slip distribution of the great 2011 Tohoku-Oki earthquake.

On the basis of the subduction zone geometry analysis carried out by Gavin Hayes *(http://earthquake.usgs.gov/earthquakes/eqinthenews/2011/usc0001xgp/)* at the United States Geological Survey, and the trench coordinates provided by [Bird, 2003], we build a fault plane divided into 240 sub-faults of 25x25 km with variable dip and strike (Fig. 6).

We use the GPS stations distributed along the Honshu Island

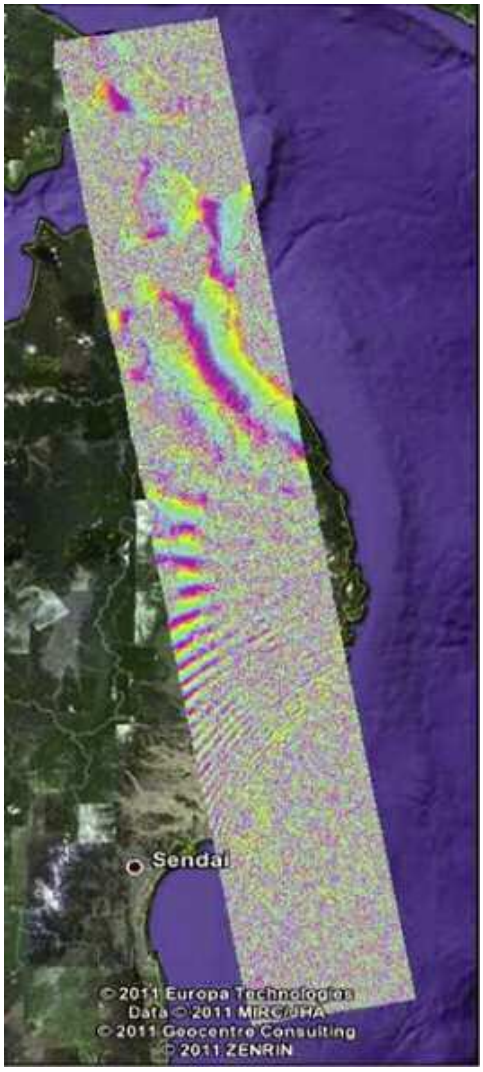

Figure 4a 28/10/2010-15/3/2011, Track 401.
Figura 4a 28/10/2010-15/3/2011, Track 401.

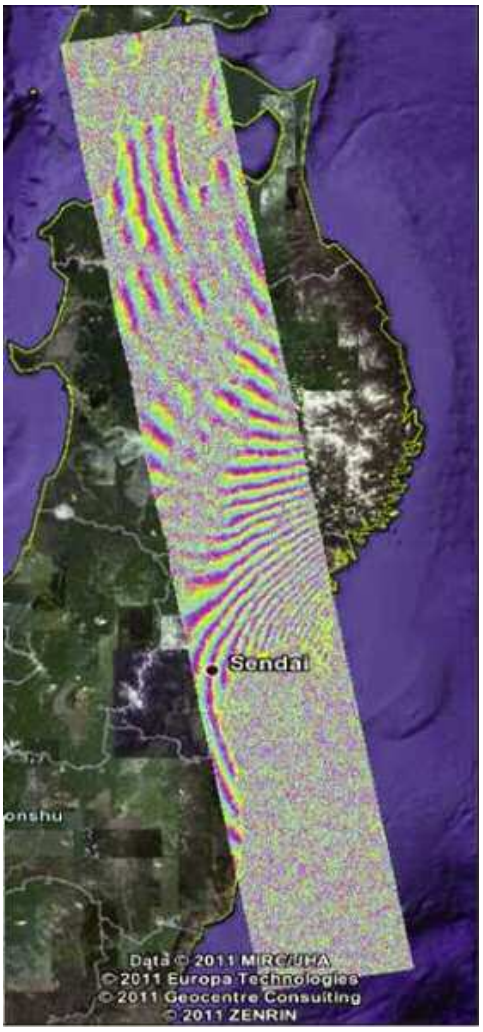

Figure 4b 29/9/2010-1/4/2011, Track 402.
Figura 4b 29/9/2010-1/4/2011, Track 402.

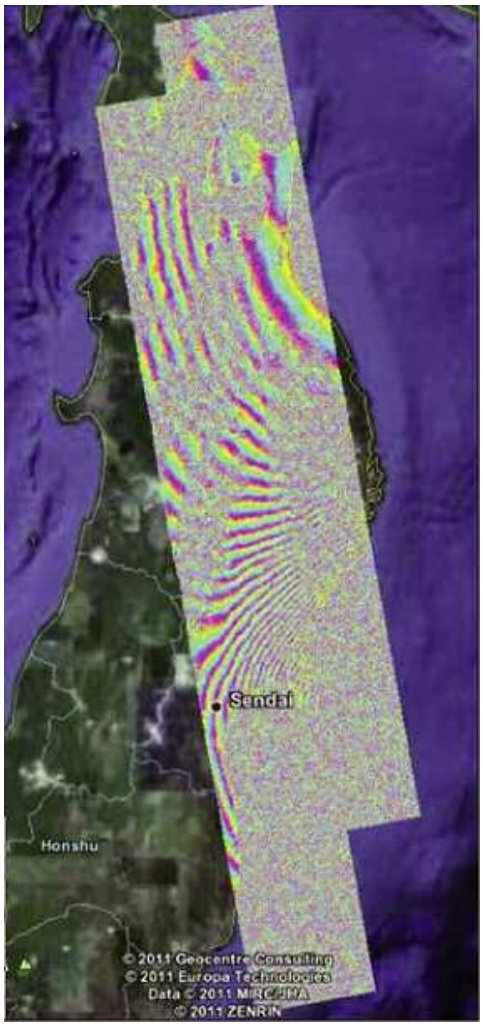

Figure 4c Combination of Tracks 401 and 402.
Figura 4c Combinazione delle Tracks 401 and 402.

that recorded a distinct coseismic deformation. All original GEONET RINEX data have been provided by the Geospatial Information Authority (GSI) of Japan and processed at INGV (Rome) with JPL's GIPSY-OASIS software, and JPL flinnR orbit and clock products. We used the kinematic precise point positioning strategy [Zumberge et al. 1997] with ambiguity resolution following the methodology described in [Bertiger et al. 2010]. Coseismic displacements are calculated as a simple difference of the position estimates averaged over 15 minutes before and after the mainshock excluding the first 5 minutes during the most intense ground shaking (Fig. 7).

We use the tsunami waveforms recorded at the ocean bottom pressure gauges (JAMSTEC) positioned off Kushiro (KPG1,2), Hatsushima (HPG1), and Muroto (MPG1,2), and those recorded at the DART buoys (NOAA) closest to the source area. We use also the DART buoys near Papua New Guinea and Philippines, in order to make the azimuthal coverage around the source as large as possible.

We calculate the Green's functions for each GPS station with the Okada's formulas [Okada, 1985].

Okada's formulas are also used to compute the vertical displacement associated with each sub-faults, which is transferred to the sea surface as the initial condition for the tsunami propagation. The propagation is calculated with COMCOT code, based on shallow water equations. We use total reflecting boundaries at the coastline and open boundaries elsewhere. Linear equations solved for the propagation. We use a grid spacing of 1 arcmin, after resampling the SRTM30_PLUS bathymetric model.

We infer the slip distribution by means of an inversion method based on global search technique (Simulated Annealing) and the linear superposition of Green's functions (e.g. [Lorito et al., 2011]).

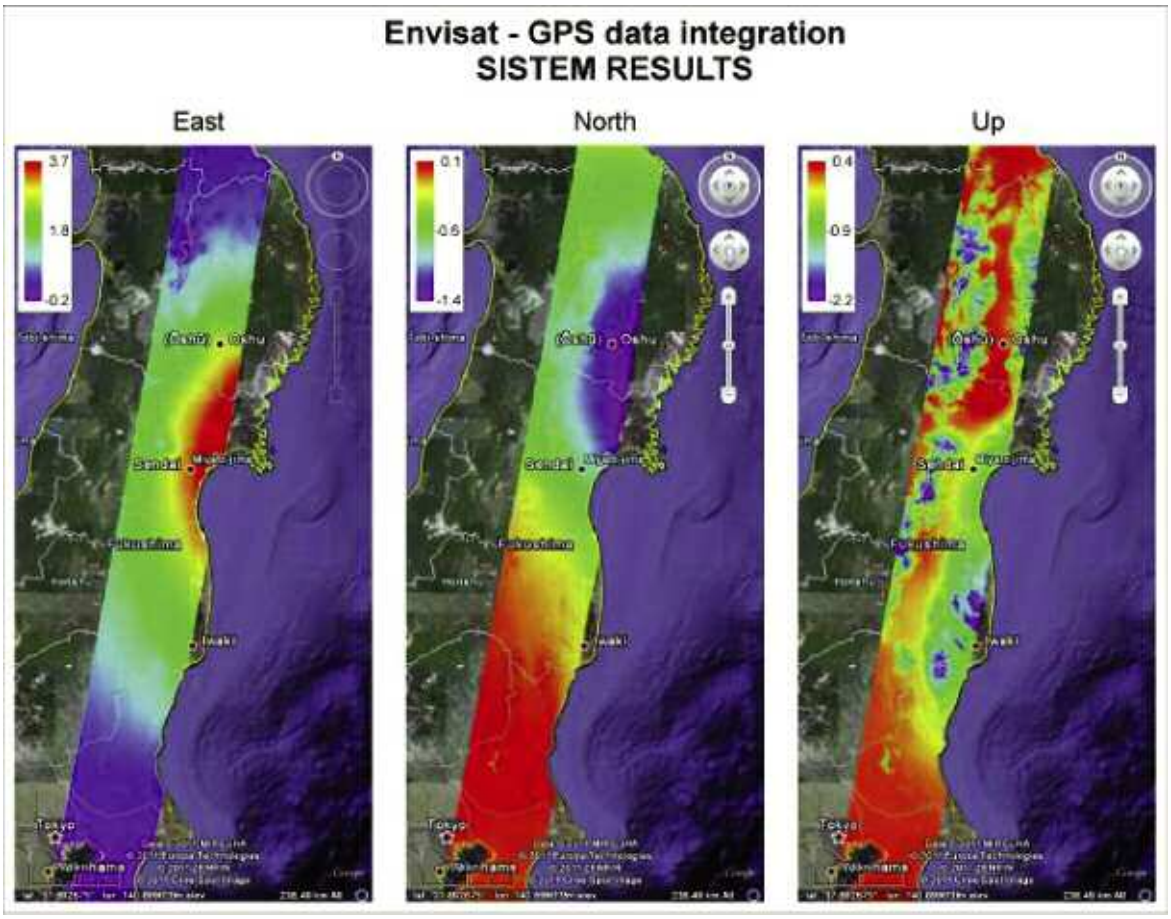

Figure 5 SISTEM results: the East, North and Up components obtained by integrating GPS and DinSAR displacements.
Figura 5 Risultato di SISTEM: componenti di spostamento Est, Nord e Verticale ottenute dalla integrazione di dati GPS e DInSAR.

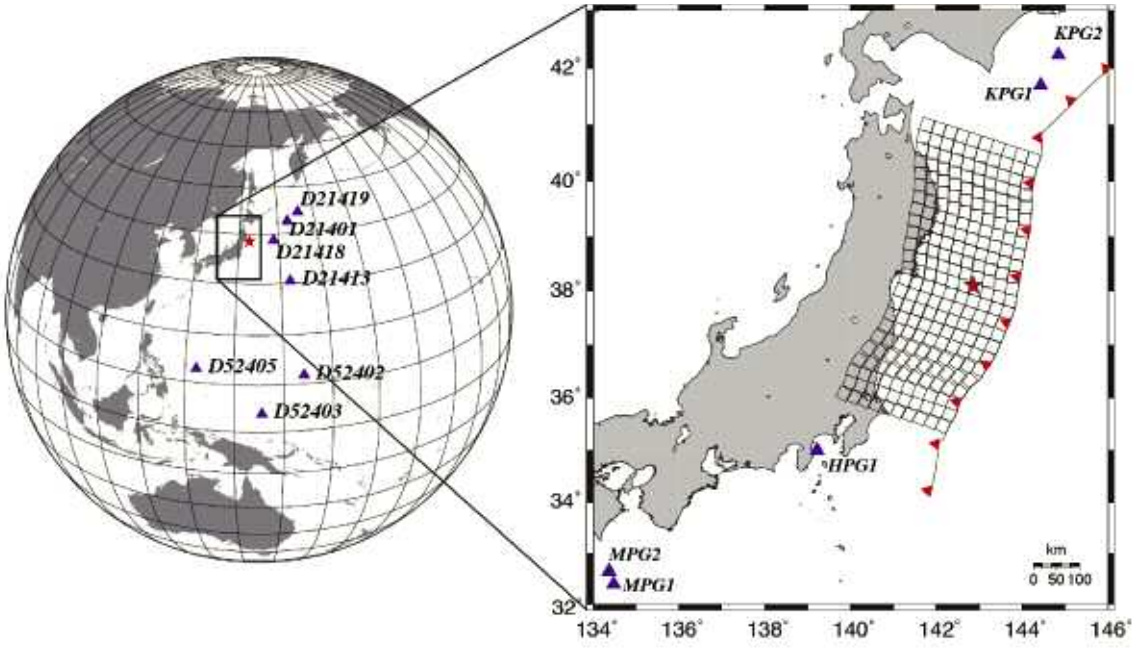

Figure 6 Location Map of the 2011 Tohoku-Oki earthquake; blue triangles represent the ocean bottom pressure gauges positions; red star represents the position of the hypocenter.
Figura 6 Mappa relative al terremoto Tohoku-Oki del 2011; i triangoli in blu le posizioni delle misure di pressione sul fondo marino; l'ipocentro è indicato dalla stella rossa.

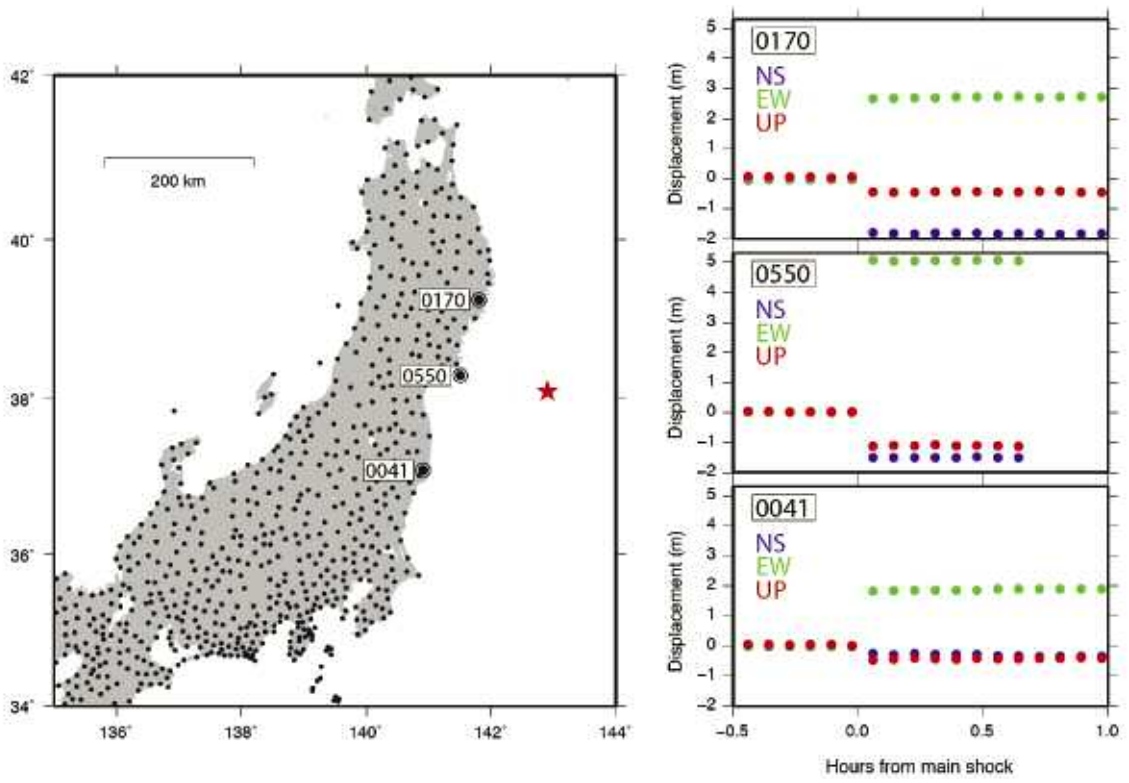

Figure 7 Location Map of the GPS stations used in this study and an example of data processing.
Figura 7 Localizzazione delle stazioni GPS utilizzate in questo lavoro e esempio di risultati delle elaborazioni.

The slip distribution of the 2011 Tohoku-Oki earthquake (Fig. 8) from joint inversion of GPS data (Fig. 9) and tsunami waveforms (Fig. 10) features a main patch of shallow slip close to the epicentre, with maximum slip values around 40 m, which explains the very high tsunami waves hitting the coast on the broadside of the rupture.

However, the first results obtained from seismological data point out a certain degree of rupture history complexity, and rupture velocity pattern might have been complicate. Differences with other preliminary inversions of seismic and geodetic data need to be further investigated.

Moreover, it will be possible to better constrain the slip distribution by using tsunameters (*Earthquake Research Institute, University of Tokyo*), ocean bottom pressure gauges (*Japan Meteorological Agency*), and even GPS buoys (*Ports and Harbours Bureau, MLIT*), which are very close and surrounding the seismic source.

A preliminary inversion to retrieve the 2011 Japan earthquake source has been done. In Fig. 11 is shown the distribution of the seismic moment release along the modeled source. We found that the total seismic moment release is 3.95e22 Nm, which corresponds to a Mw = 9.03 earthquake. This type of modeling naturally implements the seismic source in terms of seismic moment, so that the moment magnitude estimate is not biased by slip-moment conversions. The obtained preliminary model of the seismic

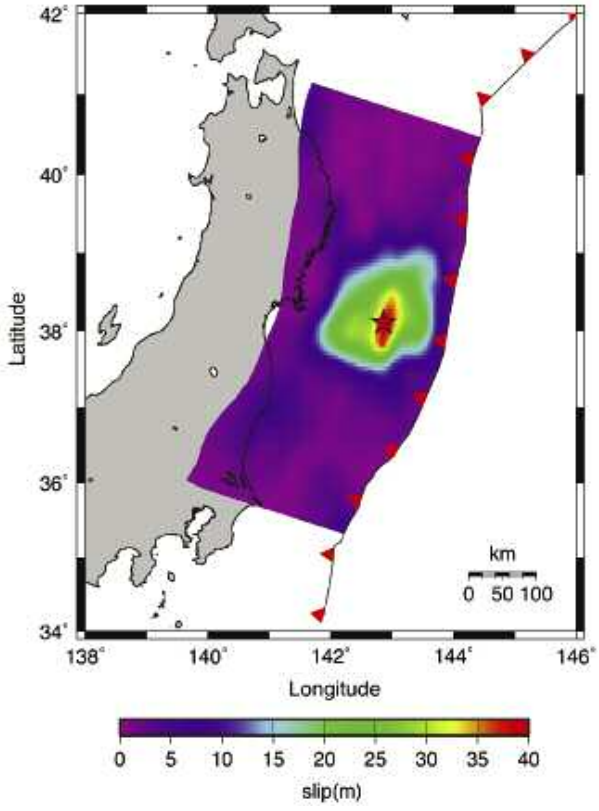

Figure 8 Slip distribution of the 2011 Tohoku-Oki earthquake from joint inversion of tsunami waveforms and GPS data.
Figura 8 Distribuzione di slip del terremoto Tohoku-Oki ottenuta dalla inversion congiunta di forme d'onda di tsunami e dati GPS.

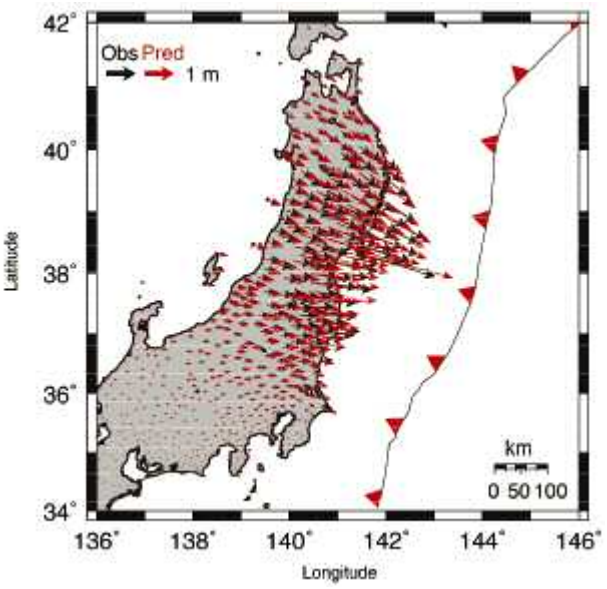

Figure 9 Comparison between observed (black) and predicted (red) GPS data.
Figura 9 Confronto tra dati GPS osservati (in nero) e modellati (in rosso).

moment release has been estimated by using GPS displacements data. A spherical self-gravitating deformation model [Melini et al., 2008] has been adopted for this purpose. The model assumes a PREM (Preliminary Reference Earth Mode) rheological layering. The fault plane geometry is fixed at USGS seismological estimates. The preliminary GPS time series are provided by the ARIA team at JPL and Caltech. All original GEONET RINEX data provided to Caltech by the Geospatial Information Authority (GSI) of Japan.

3.4 Post-seismic analysis from ERS2 InSAR

In the occasion of the Tohoku-Oki earthquake, ESA made available also data from the ERS2 satellite, previously moved on a new three days revisiting time orbit. The precise orbit files based on Laser Range data with only two days delay, have also been provided.

The optimal ERS2 orbital control allowed getting very short baseline values. These three days revisiting time means a chance to get an almost continuous monitoring system, with data and orbit files dissemination policy allowing a near-real-time data processing. Moreover, we can also extract just the coseismic deformation field with the postseismic deformation

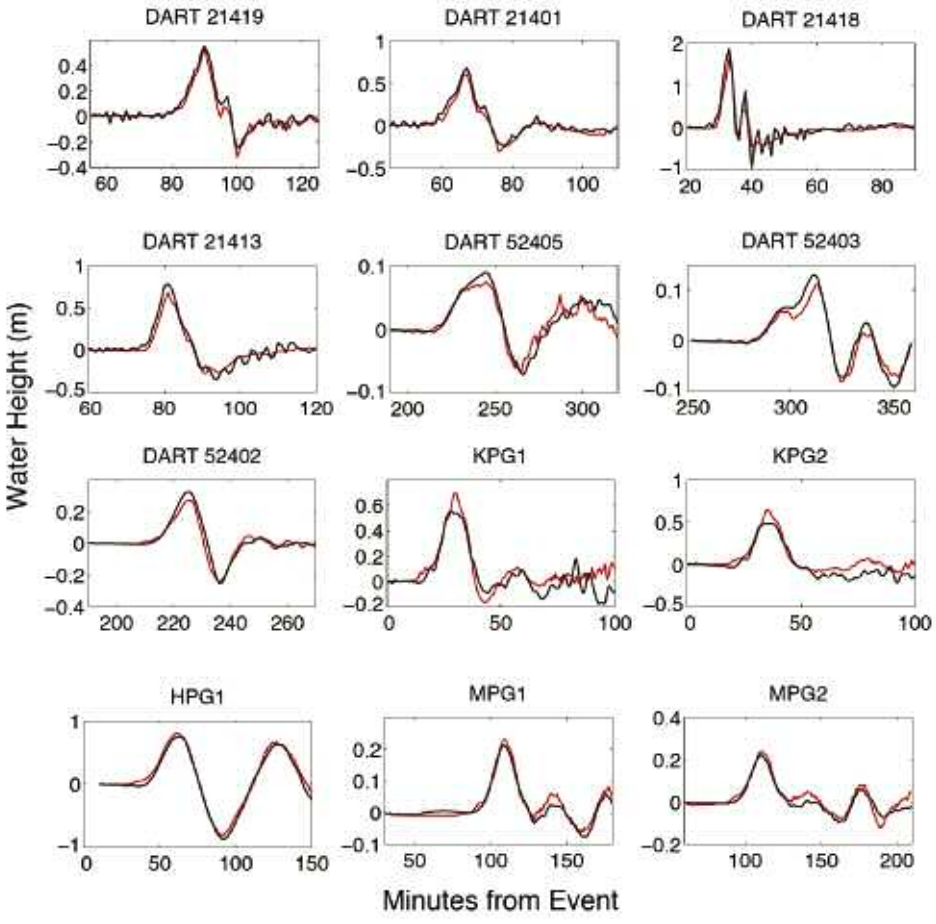

Figure 10 Comparison between observed (black) and predicted (red) tsunami waveforms.
Figura 10 Confronto tra le forme d'onda di tsunami osservate (in nero) e modellate (in rosso).

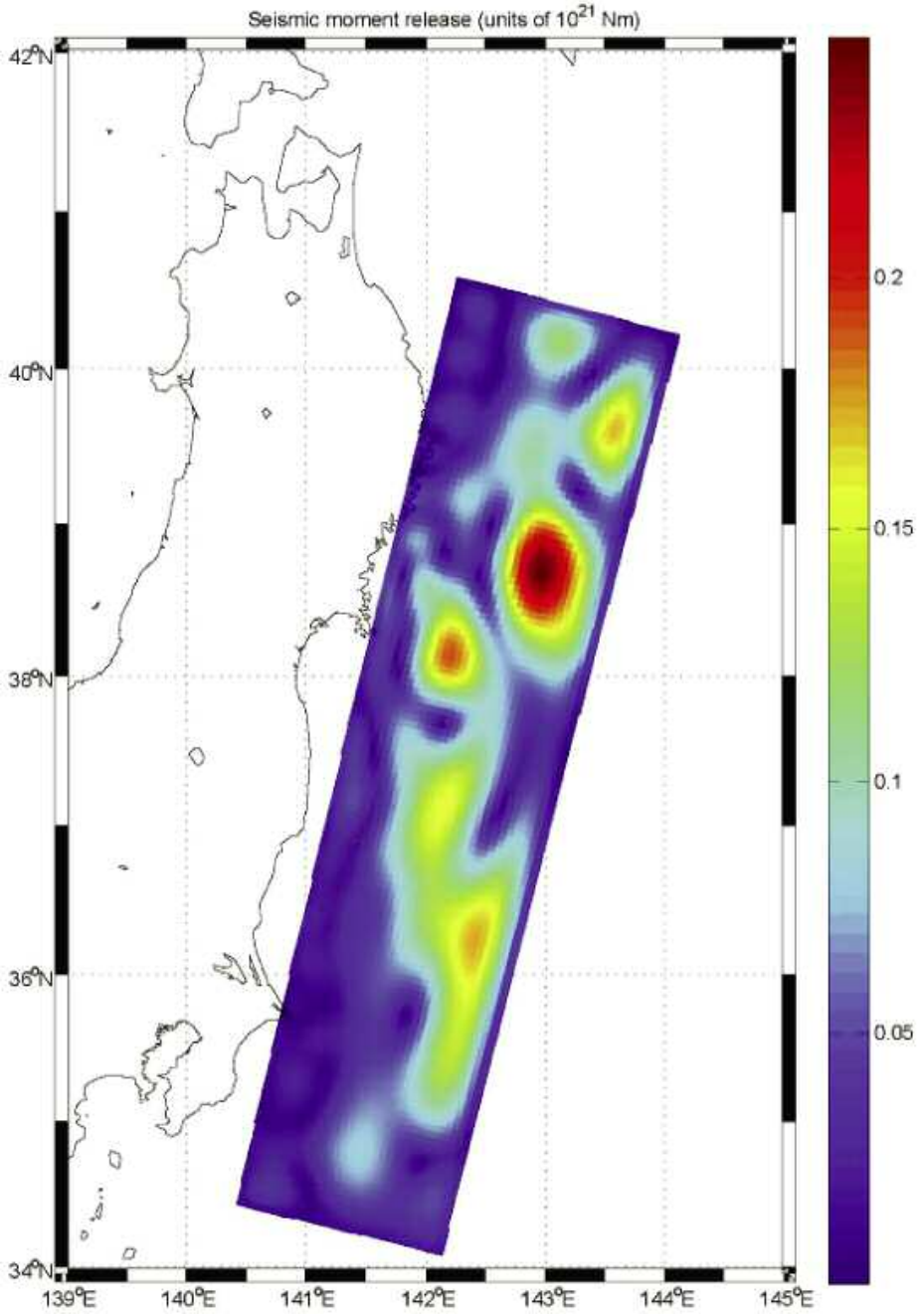

Figure 11 Preliminary inversion of seismic moment release along the 2011 Japan earthquake source. Distribution of seismic moment release along the modeled source.
Figura 11 Inversione preliminare del rilascio di momento sismico lungo la sorgente del terremoto del 2011 in Giappone. Distribuzione del rilascio di momento sismico lungo la sorgente modellata.

filtered out, unlike other spaceborne sensors with long revisiting times.

Data processing was carried out using ROI_PAC 3.0.1 *(Repeat Orbit Interferometry PACkage* – [Rosen et al, 1994] from JPL (Jet Propulsion Laboratory, USA), with all data from ascending track 24.

The choice of the ERS2 processed interferograms, has been done based also on the occurrence of some strong aftershocks (April 7th, M7.4 and May 5th, M6.3) after the mainshock of March 11st. Indeed, among the processed interferograms, in particular we analyzed the two co-seismic interferograms dated 02.04.2011-08.04.2011 and 05.05.2011-08.05.2011. From this first analysis no apparent deformation signals, associated with the events were pointed out. Probably, the displacement pattern is masked out by the atmospheric contribution.

Table 2 shows the processed interferometric pairs. Fig. 12 to Fig. 19 show the resulting interferograms.

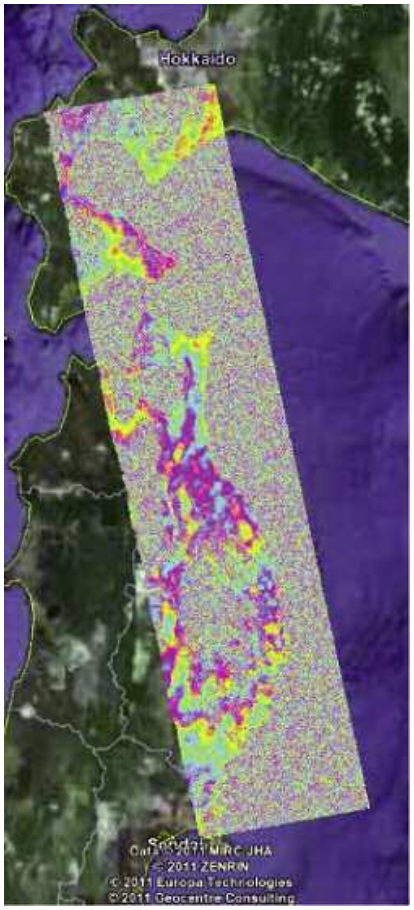

Figure 12 02.04.2011-08.04.2011.
Figura 12 02.04.2011-08.04.2011.

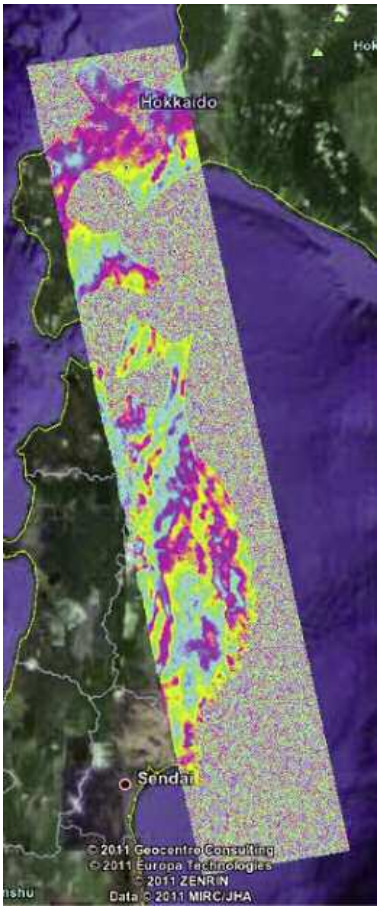

Figure 13 05.05.2011-08.05.2011.
Figura 13 05.05.2011-08.05.2011.

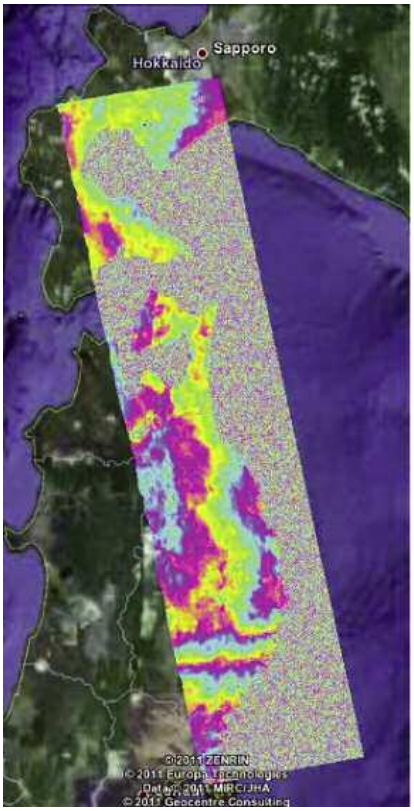

Figure 14 08.04.2011-11.04.2011.
Figura 14 08.04.2011-11.04.2011.

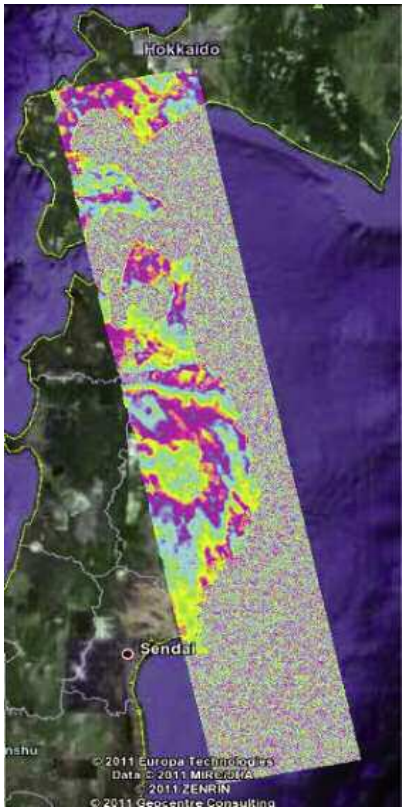

Figure 15 26.04.2011-29.04.2011.
Figura 15 26.04.2011-29.04.2011.

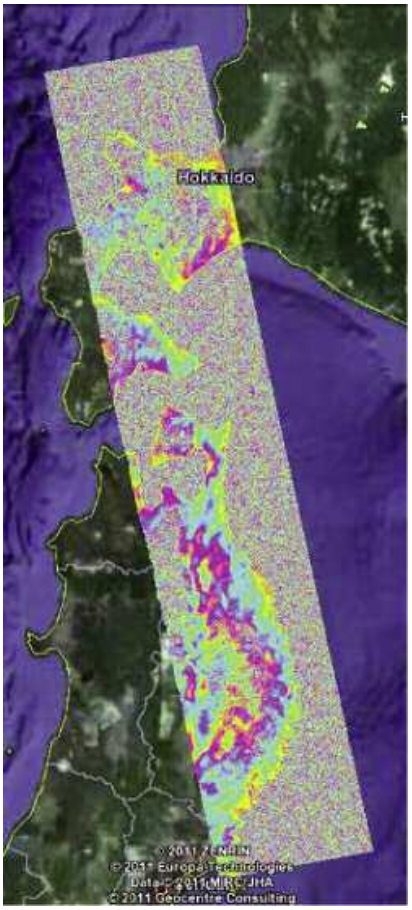

Figure 16 02.04.2011-05.04.2011.
Figura 16 02.04.2011-08.04.2011.

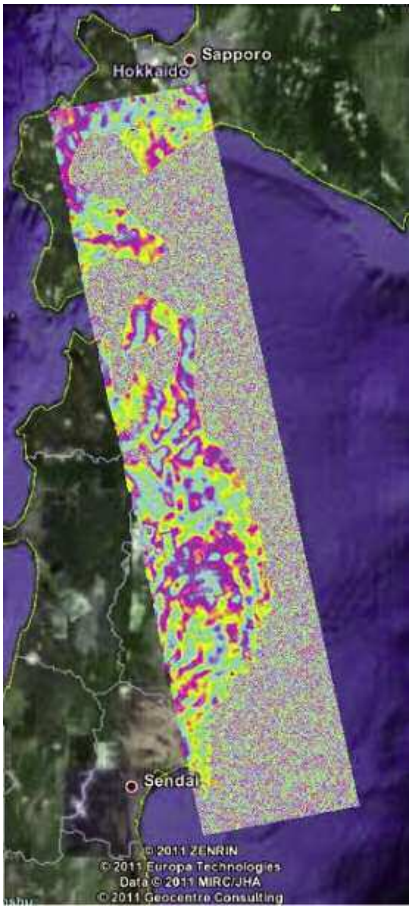

Figure 17 29.04.2011-02.05.2011.
Figura 17 29.04.2011-02.05.2011.

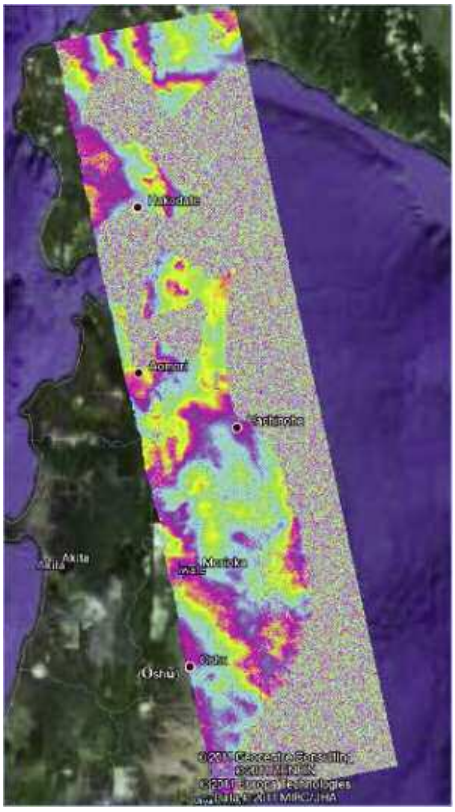

Figure 18 14.05.2011-20.05.2011.
Figura 18 14.05.2011-20.05.2011.

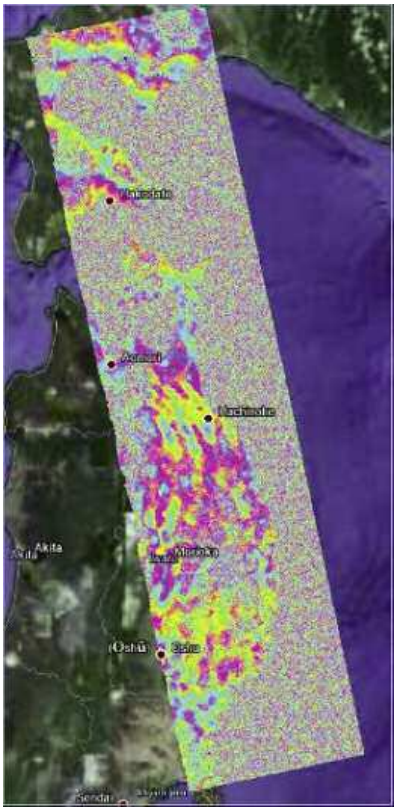

Figure 19 26.05.2011-01.06.2011.
Figura 19 26.05.2011-01.06.2011.

MASTER image	SLAVE image
02.04.2011	08.04.2011
05.05.2011	08.05.2011
08.04.2011	11.04.2011
26.04.2011	29.04.2011
02.04.2011	05.04.2011
29.04.2011	02.05.2011
14.05.2011	14.05.2011
26.05.2011	01.06.2011

Table 2 Masters and slaves dates of the ERS2 interferometric pairs.
Tabella 2 Date delle immagini ERS2 master e slave delle coppie interferometriche.

4. Surface effects of tsunami and earthquake from SAR (ALOS PALSAR) and optical (ASTER-Hyperion) sensors: inundation, landslides

The analysis of the surface effects from satellite data has been performed using a wide dataset ranging from optical images to SAR data.

4.1 ASTER data analysis

4.1.1 Sendai – Flooding

For this survey, Visible/Near-Infrared (VNIR) @15m/pixel and thermal infrared (TIR) @90m/pixel radiance images have been analyzed.
In order to characterize the effects of tsunami, we carried out a preliminary analysis by using a Decision Tree (DT) classification methodology to identify flooded areas and vegetation cover. Decision Tree has been applied to ASTER

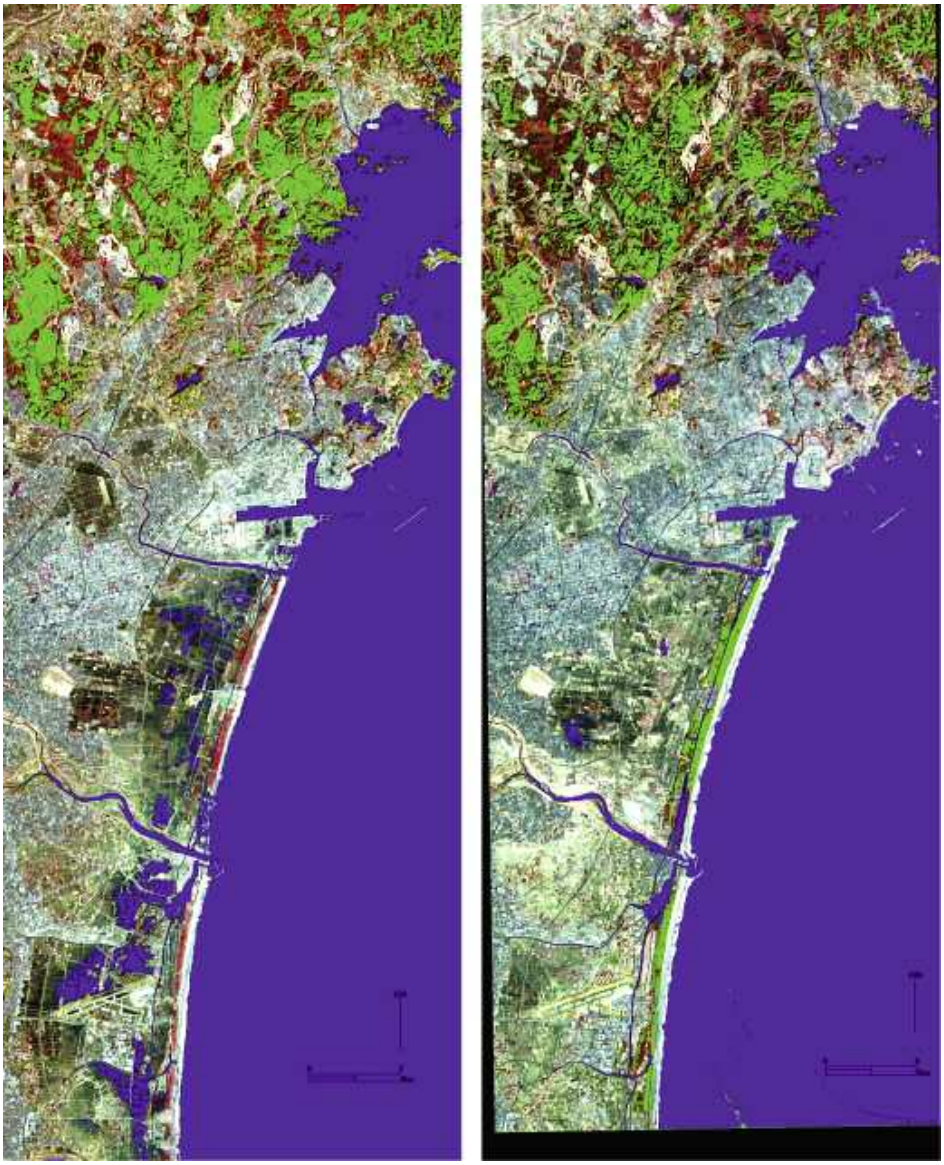

Figure 20 Sendai - ASTER VNIR color composite images left 19 March 2011, right 24 February 2011 with DT classification overlapped.
Figura 20 Sendai – imagine color composite ASTER VNIR del 19 marzo 2011 (sinistra) e del 24 febbraio 2011 (destra) con sovrapposta la classificazione DT.

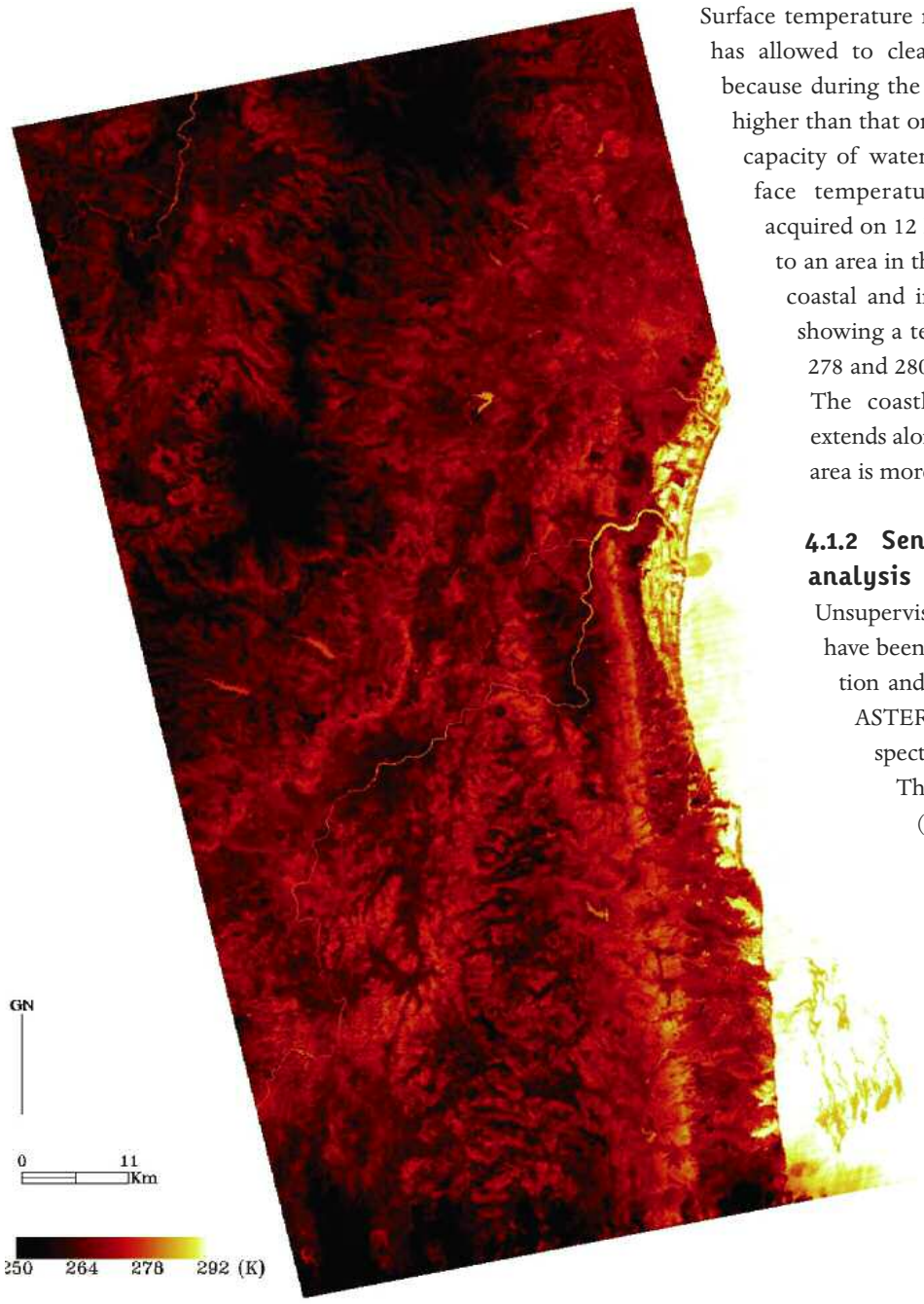

Figure 21 Sendai – ASTER TIR 12 March 2011, 12:36 UTC surface temperature (K). Sendai inland bright areas indicate flooding.
Figura 21 Sendai – temperatura superficiae (K) ASTER TIR del 12 marzo 2011, 12:36 UTC. Le aree chiare nell'entroterra di Sendai indicano l'inondato.

Surface temperature retrieval from ASTER TIR data has allowed to clearly identify the flooded areas because during the night the water temperature is higher than that one of land, due to different heat capacity of water. In Fig. 21, we report the surface temperature a night-time TIR scenes acquired on 12 March 2011, 12:36 UTC, related to an area in the south of Sendai. The flooded coastal and inland zones are clearly visible, showing a temperature ranging from about 278 and 280 K.

The coastline affected by the tsunami, extends along more than 100 km and the hit area is more than 100 km^2.

4.1.2 Sendai - Change Detection analysis

Unsupervised and supervised algorithms have been applied for land cover classification and class changes assessment using ASTER satellite images in the visible spectral range.

Three multispectral ASTER scenes (3 VNIR channels plus NDVI for each image) of the same area recorded in different dates, two pre event and one post event, treated as a single twelve-band data set, have been classified by using an unsupervised K-means classifier. The different land cover type in the Sendai area has been evaluated. The obtained result has been compared to google-earth very high resolution (VHR) optical image in order to identify which classes were corresponding to land cover changes. We focused on five change classes: flooding, debris, vegetation stress, building damage and mud plus vegetation. Fig. 22 depicts VNIR RGB images from 24 February 2011 (left), 19 March 2011 (middle) and the change detection result with the six classes overlapped on the RGB image related to 19 march 2011 (right).

VNIR scenes related to pre event and post event dates.

Fig. 20 (left panel) shows a RGB VNIR image with vegetation (green) and water (blue) pixels classified by DT. Despite the fact that the image refers to an acquisition of eight days later we can clearly see the effects of the tsunami and how much it penetrated inland reaching 5 km in the airport area. Fig. 20 (right panel) shows the DT classification of a VNIR scene related to a pre event date (24 February 2011). It highlights that the vegetation present on coastal areas has been completely destroyed by the tsunami.

4.1.3 Fukushima -Thermal analysis

In Fig. 23 is shown a surface temperature image retrieved from ASTER image of 19 March 2011, 12:42 UTC, which covers the Nuclear Power Plant of Fukushima, but it doesn't

seem to put in evidence any thermal anomaly although an oil-fired power station in the south, close to Hirono, reveals a cold spot with mean value of 278.6 K. The cold spot reveals a temperature lower than background and regards an oil tank of the plant probably as a consequence of accidents occurred after the earthquake and confirmed by the Japan Intitute of Energy and Economics which declares that the catastrophic tsunami following the earthquake seriously devastated the unit 5 coal terminal of the power station [IEEJ report, 2011].

4.1.4 Thermal Infrared data analysis from 12 March 2011 ASTER data

On March 12 2011, a night multispectral image in the Thermal Infrared spectral range, from 8 to 14 um was acquired by ASTER sensor. ASTER-TIR channel has a 90m/pixel resolution and with 5 bands between 8.13-11.65um).The interested region is southern Sendai. The TIR image has been exploited to extract the map of the floods. Despite the low resolution of the TIR channel, this derived product is relevant because it allowed defining the border of the flooding events in the south of Sendai, just one day after the tsunami.

In the image, two hot spots have also been pointed out (see Fig. 24). These two high temperature points are probably related to combustion areas.

4.2 EO-Hyperion data analysis

The area hit by the tsunami has also been imaged by a hyperspectral sensor. EO1-Hyperion acquired a scene on March 13. The EO1-Hyperion sensor, onboard NASA's EO-1 platform, is a space borne imaging spectrometer covering the wavelength region from 0.4 to 2.5 m with 220 bands at 10nm spectral resolution. The spatial resolution is 30m.

The Hyperion scene has been geocoded and atmospherically corrected by using FLAASH, a commercial tool (ITT-ENVI). VISIBLE and SWIR bands have been analyzed. In particular, this scene has been obtained by adopting a Support Vector Machine classifier. The resulting classification image is shown in Fig. 25.

The three different water classes, shown in the legend of Fig. 25, refer to different water turbidity. By Short Wavelength Infrared (SWIR , 1.1 to 2.5um) of Hyperion, and a color composite RGB, combustion- flaming areas can be detected. In this analysis, three different areas interested by combus-

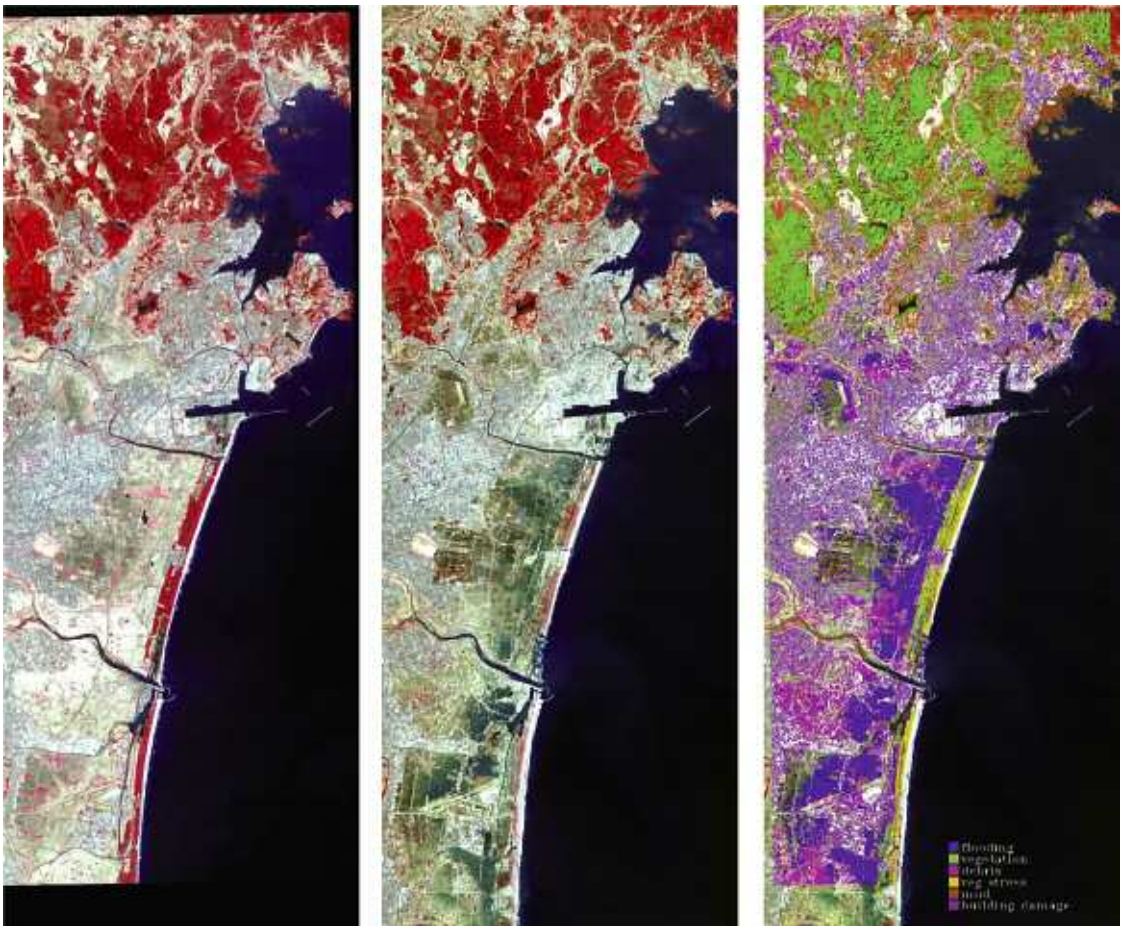

Figure 22 Sendai – ASTER VNIR 24 February 2011, 1:32 UTC (left), 19 March 2011, 12:42 UTC (middle) and land cover changes classification (right).
Figura 22 Sendai – imagine ASTER VNIR del 24 febbraio 2011, 1:32 UTC (sinistra), del 19 marzo 2011, 12:42 UTC (al centro) e classificazione dei cambiamenti del suolo (destra).

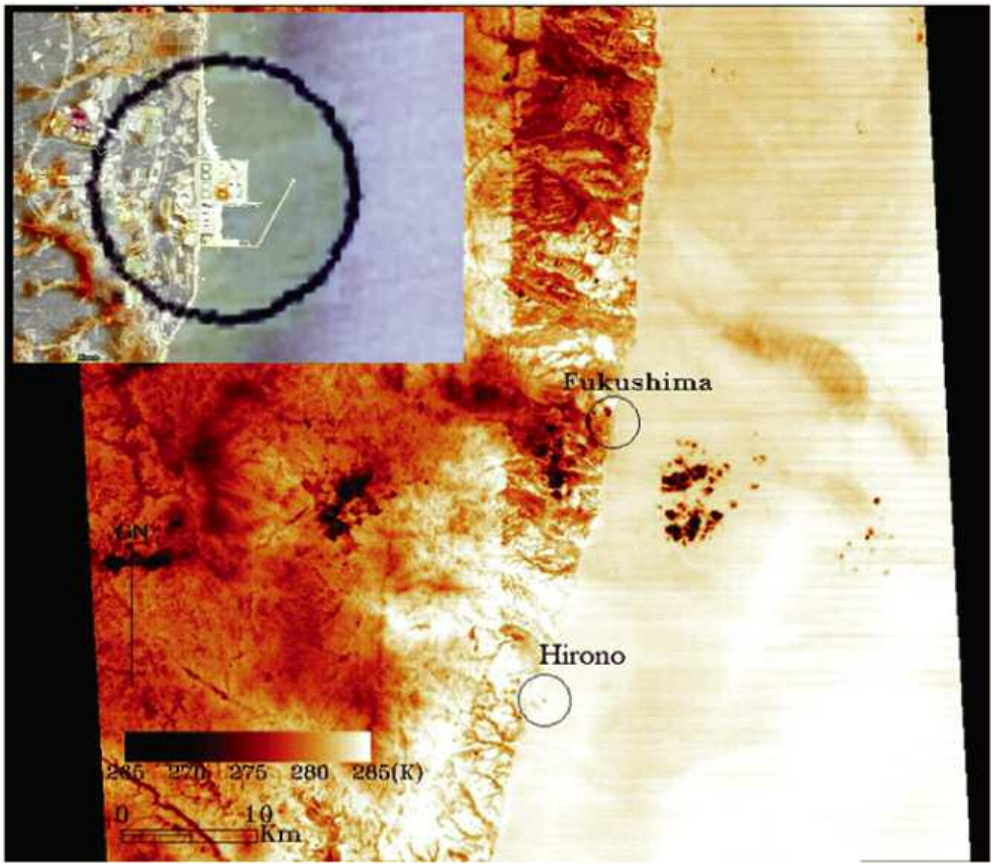

Figure 23 Fukushima – ASTER TIR 19 March 2011, 12:42 UTC surface temperature (K).The inset shows a detail indicating the cold spot onto Hirono Power Plant.
Figura 23 Fukushima –Temperatura superficiale (K) ASTER TIR del 19 marzo 2011, 12:42 UTC. Il riquadro indica un dettaglio di un punto freddo presso la centrale di Hirono.

tion events have been identified and are showed in Fig. 26. The obtained map has been validated by using the thermal image acquired by ASTER sensor on the night of March 12. In particular, an active large event is clearly shown (see section 4.1.4).

4.3 SAR data analysis

4.3.1 Sendai coastal area

ENVISAT ASAR data were also available to study the surface effect produced by the tsunami. Three images have been exploited: two before the event, on 21 November 2010 and 19 February 2011, and one post tsunami, on 21 March 2011. The backscattering value has been calculated by multi looking the data with a factor of 5x1 pixels in azimuth and range, respectively. The calibrated images have been co-registered each other and geo-coded by using the SRTM DEM. In Fig. 27 a detail of RGB color composition using pre-seismic, 19/02/2011 (Red channel), and post-seismic, 21/03/2011 (Blue and Green channels) is shown. The region of changes is represented by cyan and red colors. These areas are in agreement with flood map from ASTER thermal data. In particular, red regions correspond to zones where the open water is still present, characterized by low backscattering in the post-event image. The cyan pixels represent a higher backscattering in the post-seismic image, that can be linked to many different phenomena such as increasing of the soil moisture, presence of debris on the surface or an increasing of the roughness, all indices of an occurred change [Pulvirenti et al., 2011]. The comparison between the SAR and the thermal map in the common region allowed setting a threshold on the backscattering values for identifying the inundation limits in Sendai plain on the change image.

4.3.2 Ground subsidence in Tokyo bay

SAR data highlighted an area of coherence decay along the coastline of the Tokyo bay at Chiba prefecture. This area suffered a strong shaking. Moreover, building damages were caused by severe liquefaction occurring in the saturated sandy ground of this reclaimed land [Kishada, 2001]. Pre-seismic (21/11/2010 – 19/02/2011) and co-seismic (19/02/2011 – 21/03/2011) coherence and intensity correlation maps (Fig. 28) have been computed. The close value of perpendicular baseline, 223 m and 209 m for the pre- and the

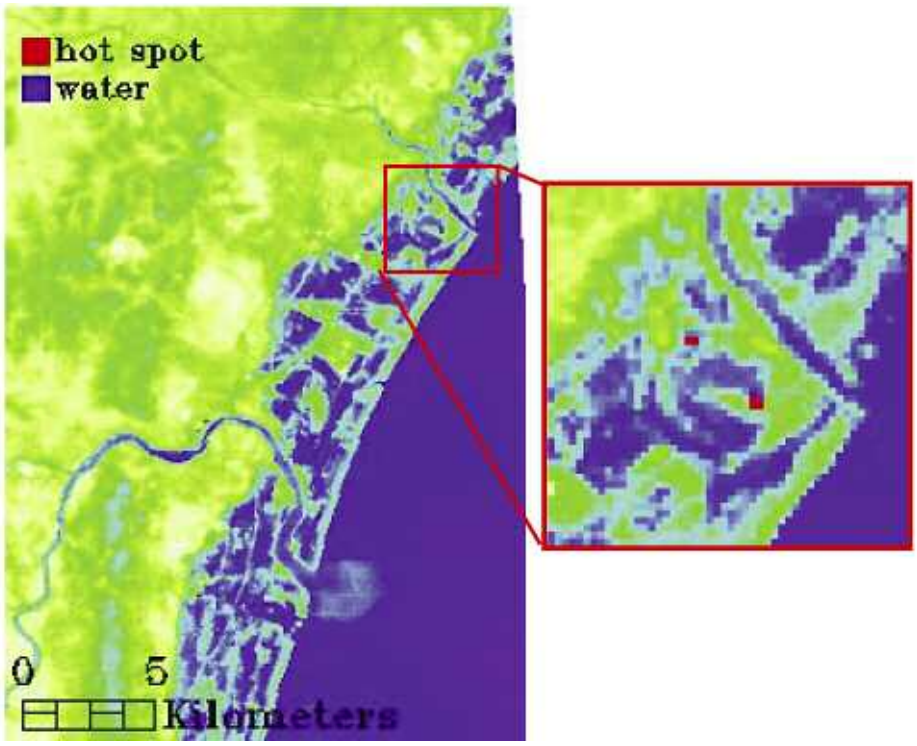

Figure 24 Flooding map from Thermal night ASTER channel acquired on MARCH 12 2011; In the red square a detail of the two hot spot is reported.
Figura 24 Mappa dell'inondato da canale termico notturno ASTER acquisito il 12 marzo 2011. Nel riquadro rosso un dettaglio di due punti caldi.

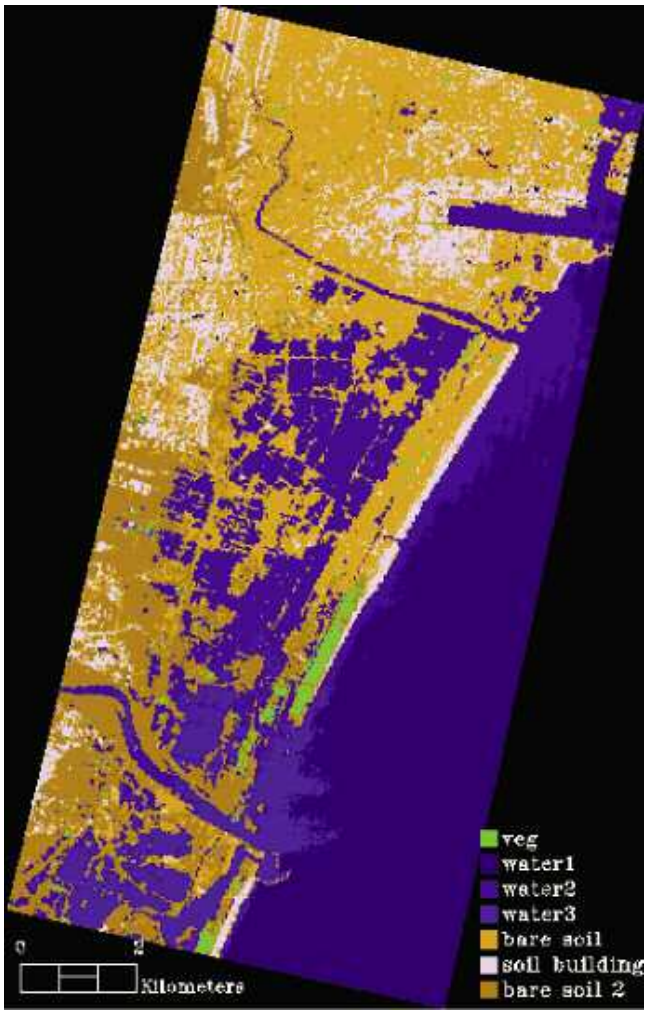

co-seismic respectively, excludes any further coherence loss, in the co-seismic one, associated to spatial decorrelation, hence the coherence loss (Fig. 28 upper panel) can be attributed to the temporal decorrelation caused by the earthquake.

The co-seismic intensity correlation (Fig. 28 lower panel) does not show an extended region of changes, but only some localized spots, where the major liquefaction effects occurred. From this analysis, we assume that the phenomenon we are observing is due to a ground subsidence resulting from the strong shaking and the pervasive liquefaction which affect the area. Indeed, the backscattering properties of the surface remain similar before and after the event, except for some restricted zones (see blue ellipses in Fig. 28) while the surface displacements is detected and gives the above mentioned coherence decay.

5. Tide gauge recordings from Mediterranean sea

Since the beginning of the instrumental age, several countries decided to establish networks of sensors devoted to sea level monitoring for navigation and scientific applications.

Figure 25 EO1-Hyperion data (30m/pixel) March 13 2011 flooding map.
Figura 25 Mappa dell'inondato da EO1-Hyperion (30m pixel) del 13 marzo 2011.

Figure 26 SWIR color composite RGB indicate two different hot spot area (1 and 2). The ASTER TIR data acquired on March 12 2011 night, has been used to validate data: two strong hot spot features on ASTER image are, weakly but still present on the EO1-Hyperion day after image (inset 1 and 2).
Figura 26 immagine color composite RGB SWIR indicante due punti caldi (1 e 2). Il dato ASTER TIR notturno acquisito il 12 marzo 2011 è stato usato per validare i dati: due punti caldi sull'immagine ASTER sono deboli ma presenti nella EO1-Hyperion il giorno seguente (riquadri 1 e 2).

After the large tsunami occurred in 1946 in the Aleutian Islands that devastated Hilo, the U.S. government started a tsunami warning capability. Only after the Chilean earthquake of 1960, which caused a tsunami that devastated Chile and killed people in the Hawaian and Japanese islands, monitoring networks were improved and the Pacific Tsunami Warning Center was created. After the 2004 Indian Ocean tsunami, additional improvement to sea level and tsunami global monitoring systems were performed, including in the Mediterranean region. This global scale infrastructure, together with national agencies and single organizations, are now able to distribute sea level recordings by internet and near real time sea level data recordings that can be easily retrieved, are often produced (IOC at global scale, http://www.ioc-sealevelmonitoring.org/ and ISPRA for the Italian region http://www.mareografico.it/).
At the time of the March 11th, 2011, M 9.0 Tohoku-Oki earthquake, were available on line tide gauge data from about 200 stations. Part of them are located in the Mediterranean. In this report we show and discuss the results from the analysis of a set of stations located in the near field of the earthquake epicenter (Fig.29) and in the Mediterranean basin. Although the Mediterranean sea is far away from the earthquake source of March 11, 2011 earthquake and it is about a closed basin, the tide gauge data show a signal that can be addressed to a sea level change induced by this event (Fig. 30 and Fig. 31).

5.1 Data analysis

The analyzed data set consists of tidal recordings from about 200 available tide gauge stations. About 90 of these are located in the Oceans, while about 110 in the Mediterranean basin. The latter includes the Italian tide gauge network consisting in 30 stations. We have retrieved or obtained sea level data from IOC (http://www.ioc-sealevelmonitoring.org/), ISPRA (http://www.mareografico.it/) and PSMSL (www.pol.ac.uk). As our study aims to estimate eventual tsunami effects in remote seas from the earthquake epicenter, we have mainly focused on the tidal recordings for the Mediterranean region. Tidal data, after applying an inverse

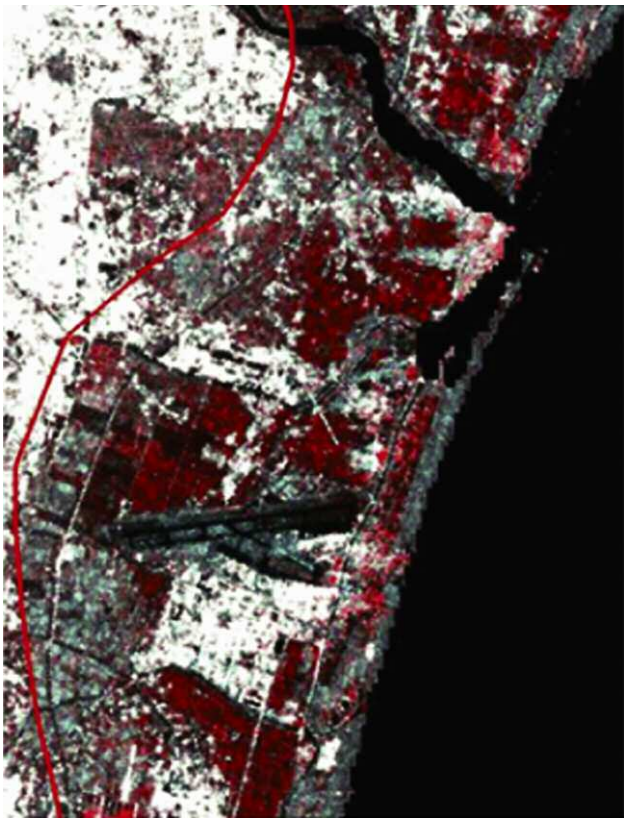

Figure 27 RGB color composite of two SAR backscattering images (R: 19/02/2011; G: 21/03/2011; B: 21/03/2011). In red and cyan are highlighted the areas of changes. Red continuos line is the estimated inundation limit.
Figura 27 RGB color composite di due immagini SAR (R: 19/02/2011; G: 21/03/2011; B: 21/03/2011). Le aree affette da cambiamenti sono evidenziate in rosso e ciano. La linea rossa continua mostrail limite stimato dell'inondato.

barometric correction, have been analyzed through an advanced filtering technique that decomposes a non-stationary time series X(t) through oscillating modes (see e.g., [Huang et al.1998], [Vecchio et al. 2010]). These are not obtained a priori but empirically calculated from the time series under analysis. In this way we are able to properly identify the contributions at different timescales to the tide variations. In particular, we focus on T(t), namely the contribution to the tide signal at time scales greater than 12 hours, describing the dynamical behavior of low-frequency processes and trends.

Fig. 30 and Fig. 31 show two examples of the sea level time history for two different stations located at S. Benedetto and Livorno (time is measured as lag from the time of the M = 8.9 Japan earthquake, t = 0, is the time of the earthquake, here and in the following Figures). The dynamics of the T(t) function (red curve), obtained through the filtering procedure, is overplotted. T(t) shows a peak at a time of 38 hours after the earthquake, which is connected to a positive perturbation of the sea level, likely due to the wave crossing the Mediterranean, along longer time scales. Tidal data from tide gauge stations located in the Oceans and the Mediterranean were analyzed. Results show that the Mediterranean basin is sensitive to far large earthquakes capable to generate giant tsunamis, such the case of the March 11th, 2011, M 8.9 Tohoku-Oki earthquake, occurred offshore the Honshu island (Japan). The diurnal and semidiurnal tides recorded at the tide gauge stations located in the Mediterranean were disturbed both in amplitude and frequency.

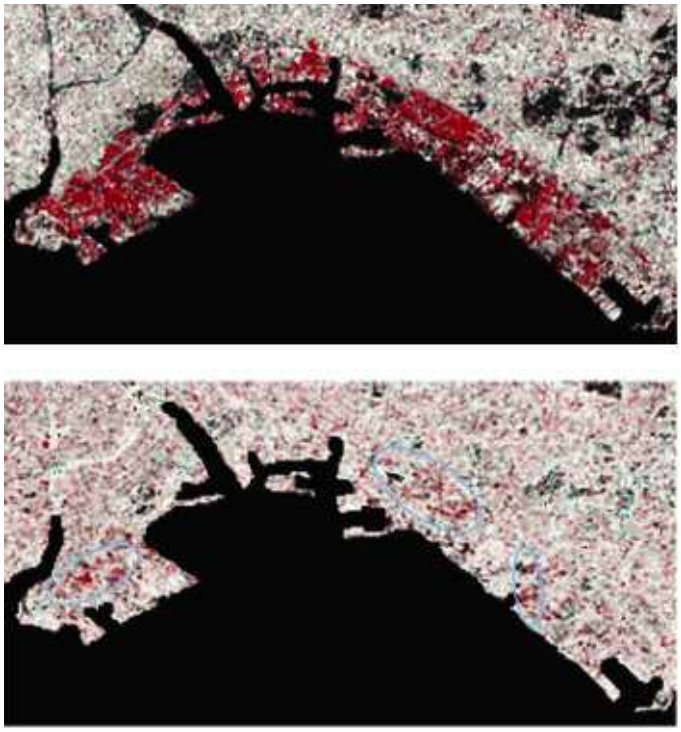

Figure 28 Upper panel shows a RGB color composite of two SAR coherence images, R=Pre-seismic (21/11/2010-19/02/2011); G=Co-seismic (19/02/2011-21/03/2011); B=Co-seismic (19/02/2011-21/03/2011); Lower panel shows a RGB color composite of two SAR intensity correlation images, R=Pre-seismic (21/11/2010-19/02/2011), G=Co-seismic (19/02/2011-21/03/2011); B=Co-seismic (19/02/2011-21/03/2011); the blue ellipses represent the decorrelation due to major surface liquefaction effects, which are in accordance with [Kishada, 2001].
Figura 28 (in alto) RGB color composite di due immagini SAR di coerenza R=Pre-sismica (21/11/2010-19/02/2011); G=Co-sismica (19/02/2011-21/03/2011); B=Co-sismica (19/02/2011-21/03/2011); (in basso) RGB color composite di due immagini SAR di correlazione R=Pre-sismica (21/11/2010-19/02/2011), G=Co-sismica (19/02/2011-21/03/2011); B=Co-sismica (19/02/2011-21/03/2011); le ellissi blu mostrano la decorrelazione dovuta a effetti di liquefazione del suolo, in accordo con [Kishada, 2001].

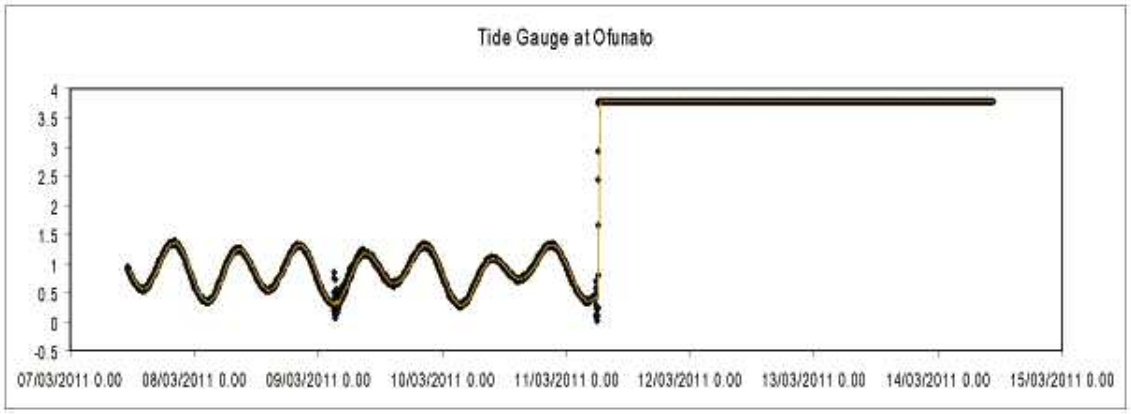

Figure 29 Tidal signal at the near field station of Ofunato (Japan). The onset of the tsunami waves at this station saturated the recordings.
Figura 29 Segnale di marea presso la stazione di Ofunato (Giappone). L'inizio dell'onda di tsunami presso questa stazione ha saturato le registrazioni.

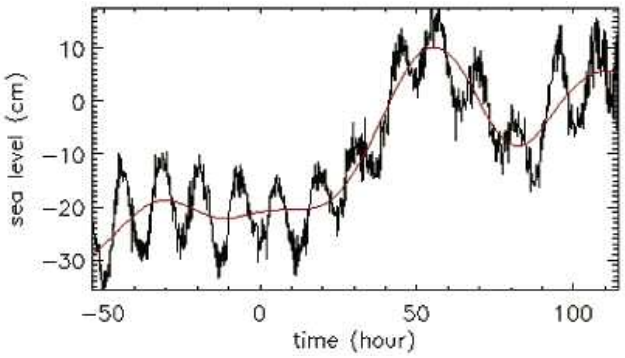

Figure 30 Time history of the sea level at S. Benedetto (black line) along with the long frequency contribution (red line).
Figura 30 Serie temporale del livello del mare presso S. Benedetto (linea near) con il contributo in frequenza (linea rossa).

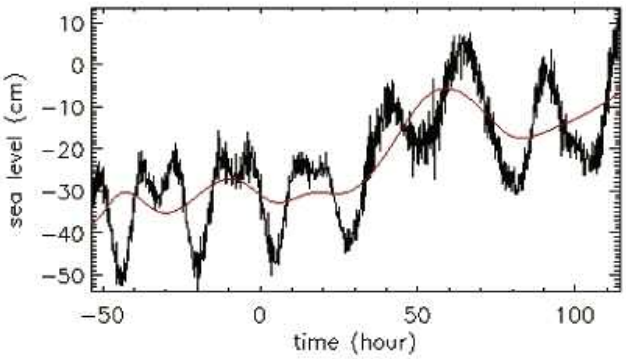

Figure 31 Time history of the sea level at Livorno (black line) along with the long frequency contribution (red line).
Figura 31 Serie temporale del livello del mare presso Livorno (linea nera) con il contributo in frequenza (linea rossa).

Acknowledgments

We thank Dave Pieri from JPL for ASTER data supply.

References

Bertiger, W., S. Desai, B. Haines, N. Harvey, A. Moore, S. Owen, and J. Weiss, (2010). *Single receiver phase ambiguity resolution with GPS data*, J. Geodesy, 84, 327-337, doi:10.1007/s00190-010-0371-9.

Bird, P., (2003). *An updated digital model of plate boundaries*, Geochem. Geophys. Geosyst. 4, 1027.

Guglielmino G., Nunnari G., Puglisi G., Spata A., (2011). *Simultaneous and Integrated Strain Tensor Estimation from geodetic and satellite deformation Measurements (SISTEM) to obtain three-dimensional displacements maps*, IEEE Trans. Geosc. Rem. Sens., vol. 49, 1815-1826, doi: 10.1109/TGRS.2010.2103078.

Institute of Energy Economics, Japan (2011). *Impact of Great East Japan Earthquake on Coal Thermal Power Generation and Coal Demand, June 2011*, available on line at http://eneken.ieej.or.jp/data/3896.pdf.

Kishida, T., (2011). *Phase 1: Liquefaction Damages on Reclamation Lands In Chiba Bay Area After Tohoku Pacific Coast Earthquake On March 11, 2011*, available online at freesia.arch.ues.tmu.ac.jp/TohokuEQ2011/201103/msg48.1.pdf.

Lorito, S., F. Romano, S. Atzori, X. Tong, A. Avallone, J. McCloskey, M. Cocco, E. Boschi, A. Piatanesi, (2011). *Limited overlap between the seismic gap and coseismic slip of the great 2010 Chile earthquake*, Nature Geoscience, 10.1038/NGEO1073, 4(3), 173-177.

Melini, D., Cannelli, V., Piersanti, A. and Spada, G., (2008). *Post-seismic rebound of a spherical Earth: new insights from the application of the Post–Widder inversion formula*, Geophysical Journal International, 174: 672–695. doi: 10.1111/j.1365-246X.2008.03847.

Okada, Y. (1985). *Surface deformation due to shear*, Bull. Seismol. Soc. Am. 75, 1135–1154.

Pulvirenti, L., Pierdicca, N., Chini M., and Guerriero L., (2011). *An algorithm for operational flood mapping from Synthetic Aperture Radar (SAR) data based on the fuzzy logic*, Natural Hazards and Earth System Sciences, vol. 11, pp. 529-540.

Rosen, P. A., S. Hensley, G. Peltzer, and Simons M., (2004). *Updated repeat orbit interferometry package released*, Eos Trans. AGU, 85(5), 47, doi:10.1029/2004EO050004.

Zumberge, J. F., M. B. Heflin, D. C. Jefferson, M. M. Watkins, F. H. Webb, (1997). *Precise point positioning for the efficient and robust analysis of GPS data from large networks*, J. Geophys. Res., 102 (B3), 5005-5017.

Summary

Coordinamento editoriale e impaginazione
Centro Editoriale Nazionale | INGV

Progetto grafico e redazionale
Daniela Riposati | Laboratorio Grafica e Immagini | INGV

Via di Vigna Murata, 605
00143 Roma
Tel. +39 06518601 Fax +39 065041181

http://www.ingv.it

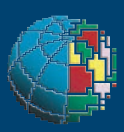

Istituto Nazionale di Geofisica e Vulcanologia